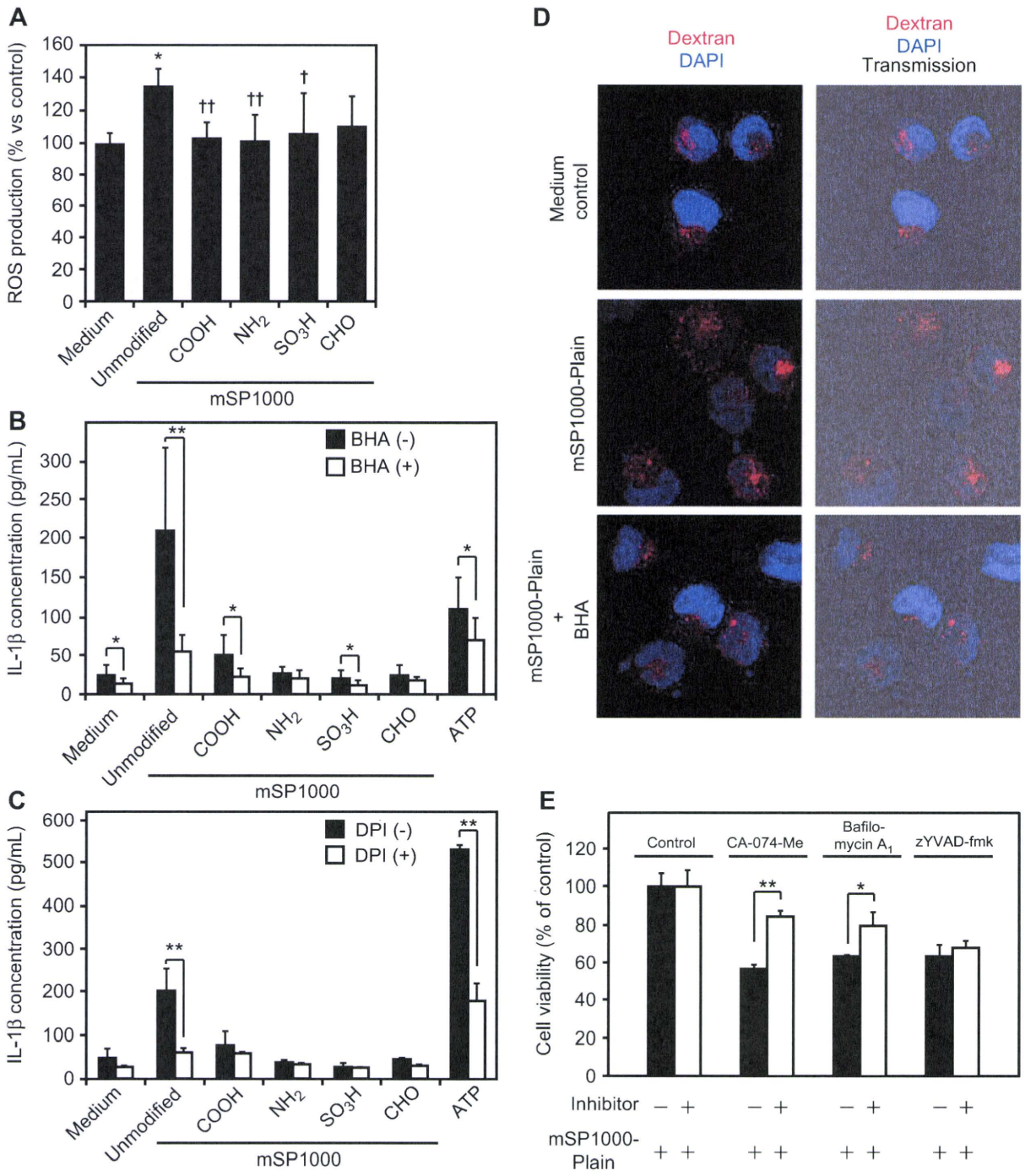

Fig. 6. Unmodified mSP1000–induced ROS production induces endosomal rupture and subsequent IL-1β production. (A) ROS production levels in PMA-primed THP-1 cells. Cells were treated with each type of mSP1000 for 24 h and incubated with H_2DCFDA (10 μM) for 45 min. Fluorescence was then measured at $OD_{485-530}$. ROS production intensity was calculated by the formula ROS production intensity = fluorescence/number of live cells. ROS production intensity of untreated control cells was arbitrarily set to 100%. Data represent means ± SD ($n = 5$; $^{*}P < 0.05$ versus value for PBS control, $^{\dagger}P < 0.05$, $^{\dagger\dagger}P < 0.01$ versus value for unmodified mSP1000, ANOVA). (B, C) Involvement of ROS in mSP1000-induced IL-1β production. PMA-primed THP-1 cells were treated with each type of mSP1000 or with ATP for 6 h in the absence (black bars) or presence (white bars) of (B) BHA (150 μM) or (C) DPI (60 μM), and IL-1β production levels were measured by ELISA. (D) Confocal microscopy of endosomal morphology. PMA-primed THP-1 cells were incubated with Alexa Fluor 594–conjugated dextran (red) and unmodified mSP1000 for 6 h in the presence (bottom) or absence (middle) of BHA (150 μM). Cells were then observed by confocal microscopy. Arrows indicate cells with spread of dextran into the cytoplasm. (E) Involvement of cathepsin B and caspase-1 in unmodified mSP1000–induced cytotoxicity. PMA-primed THP-1 cells were treated with unmodified mSP1000 for 24 h in the absence (black bars) or presence (white bars) of CA-074-Me (2 μM), bafilomycin A_1 (250 nM), or zYVAD-fmk (10 μM). Cell viability was measured by methylene blue assay. Data represent means ± SD ($n = 5$; $^{*}P < 0.05$, $^{**}P < 0.01$ versus value for inhibitor [−] control within each treatment pair, *t*-test).

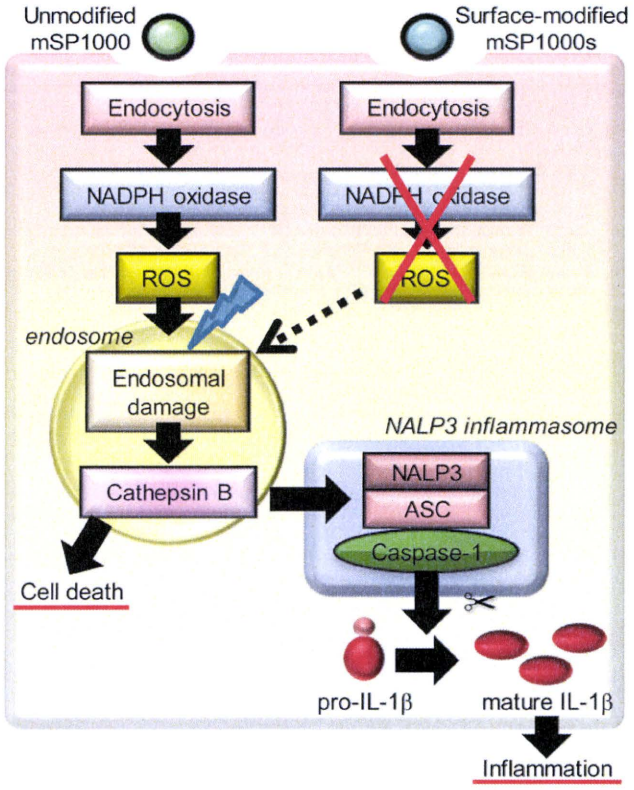

Fig. 7. Model of mSP1000-induced IL-1β maturation pathways. Unmodified mSP1000–induced IL-1β maturation is mediated by phagocytosis, activation of NADPH oxidase, ROS production, endosomal rupture, active cathepsin B leakage, assembly of NALP3 inflammasome, and caspase-1 activation. Surface-modified mSP1000s do not activate NADPH oxidase or ROS production, although they are taken up at the same rate as unmodified mSP1000.

dependent on cathepsin B (Fig. 6E) with the ASC assembly (Fig. 4), which means that unmodified mSP1000–induced cell death might occur by pyronecrosis. Pyronecrosis is considered to elicit substantial inflammation and to affect the local environment, whereas apoptosis is widely accepted as non-inflammatory cell death without effects around the dying cells [48]. Thus, pyronecrosis is likely to contribute substantially to the disease state in patients with inflammatory diseases.

We revealed here that SP-induced ROS act as an important upstream signal in the NLRP3 activation pathway. Moreover, we showed that modification of mSP1000s with functional groups suppressed their inflammatory effects. We have since obtained similar results with nanosized particles (nSP70) (unpublished data). These results support our hypothesis that appropriate surface modification of SPs suppresses their inflammatory effect. However, we speculate that blind modification could exacerbate the inflammatory effect, and we consider that an analysis of the mechanisms of the phenomena reported here is necessary.

5. Conclusions

We reveal here that unmodified mSP1000–induced IL-1β production is mediated by the activation of NADPH oxidase, ROS production, endosomal rupture, active cathepsin B leakage, assembly of NLRP3 inflammasome, and caspase-1 activation. Furthermore, by surface modification with functional groups, we successfully suppressed unmodified mSP1000–induced ROS production, an upstream signal in the NLRP3 activation pathway, and the subsequent inflammatory responses or cell death. We consider that further studies of the relationship between surface characteristics and biological effects would lead to the development of safe and effective SPs.

Acknowledgements

The authors declare that they have no conflict of interests. We thank Dr. D.T. Golenbock (Department of Infectious Diseases and Immunology, University of Massachusetts Medical School) for providing CFP–ASC plasmid. This study was supported in part by grants from the Ministry of Health, Labor, and Welfare of Japan; by the Ministry of the Environment of Japan; and by the Global COE Program "In Silico Medicine" at Osaka University.

Appendix

Figures with essential color discrimination. Figs. 2, 4–7 in this article are difficult to interpret in black and white. The full color images can be found in the on-line version, at doi:10.1016/j.biomaterials.2010.05.036.

References

[1] Mossman BT, Churg A. Mechanisms in the pathogenesis of asbestosis and silicosis. Am J Respir Crit Care Med 1998;157:1666–80.
[2] Huaux F. New developments in the understanding of immunology in silicosis. Curr Opin Allergy Clin Immunol 2007;7:168–73.
[3] Hirsch LR, Stafford RJ, Bankson JA, Sershen SR, Rivera B, Price RE, et al. Nanoshell-mediated near-infrared thermal therapy of tumors under magnetic resonance guidance. Proc Natl Acad Sci U S A 2003;100:13549–54.
[4] Bharali DJ, Klejbor I, Stachowiak EK, Dutta P, Roy I, Kaur N, et al. Organically modified silica nanoparticles: a nonviral vector for in vivo gene delivery and expression in the brain. Proc Natl Acad Sci U S A 2005;102:11539–44.
[5] Roy I, Ohulchanskyy TY, Bharali DJ, Pudavar HE, Mistretta RA, Kaur N, et al. Optical tracking of organically modified silica nanoparticles as DNA carriers: a nonviral, nanomedicine approach for gene delivery. Proc Natl Acad Sci U S A 2005;102:279–84.
[6] Bottini M, D'Annibale F, Magrini A, Cerignoli F, Arimura Y, Dawson MI, et al. Quantum dot-doped silica nanoparticles as probes for targeting of T-lymphocytes. Int J Nanomedicine 2007;2:227–33.
[7] Verraedt E, Pendela M, Adams E, Hoogmartens J, Martens JA. Controlled release of chlorhexidine from amorphous microporous silica. J Contr Release 2010;142:47–52.
[8] Wiethoff AJ, Reed KL, Webb TR, Warheit DB. Assessing the role of neutrophil apoptosis in the resolution of particle-induced pulmonary inflammation. Inhal Toxicol 2003;15:1231–46.
[9] Cho WS, Choi M, Han BS, Cho M, Oh J, Park K, et al. Inflammatory mediators induced by intratracheal instillation of ultrafine amorphous silica particles. Toxicol Lett 2007;175:24–33.
[10] Park EJ, Park K. Oxidative stress and pro-inflammatory responses induced by silica nanoparticles in vivo and in vitro. Toxicol Lett 2009;184:18–25.
[11] Akerman ME, Chan WC, Laakkonen P, Bhatia SN, Ruoslahti E. Nanocrystal targeting in vivo. Proc Natl Acad Sci U S A 2002;99:12617–21.
[12] Kirchner C, Liedl T, Kudera S, Pellegrino T, Munoz Javier A, Gaub HE, et al. Cytotoxicity of colloidal CdSe and CdSe/ZnS nanoparticles. Nano Lett 2005;5:331–8.
[13] Dostert C, Petrilli V, Van Bruggen R, Steele C, Mossman BT, Tschopp J. Innate immune activation through Nalp3 inflammasome sensing of asbestos and silica. Science 2008;320:674–7.
[14] Albrecht C, Schins RP, Hohr D, Becker A, Shi T, Knaapen AM, et al. Inflammatory time course after quartz instillation: role of tumor necrosis factor-alpha and particle surface. Am J Respir Cell Mol Biol 2004;31:292–301.
[15] He X, Nie H, Wang K, Tan W, Wu X, Zhang P. In vivo study of biodistribution and urinary excretion of surface-modified silica nanoparticles. Anal Chem 2008;80:9597–603.
[16] Waters KM, Masiello LM, Zangar RC, Tarasevich BJ, Karin NJ, Quesenberry RD, et al. Macrophage responses to silica nanoparticles are highly conserved across particle sizes. Toxicol Sci 2009;107:553–69.
[17] Dinarello CA. Interleukin-1 beta, interleukin-18, and the interleukin-1 beta converting enzyme. Ann N Y Acad Sci 1998;856:1–11.
[18] Petrilli V, Dostert C, Muruve DA, Tschopp J. The inflammasome: a danger sensing complex triggering innate immunity. Curr Opin Immunol 2007;19:615–22.

[19] Cassel SL, Eisenbarth SC, Iyer SS, Sadler JJ, Colegio OR, Tephly LA, et al. The Nalp3 inflammasome is essential for the development of silicosis. Proc Natl Acad Sci U S A 2008;105:9035–40.
[20] Hornung V, Bauernfeind F, Halle A, Samstad EO, Kono H, Rock KL, et al. Silica crystals and aluminum salts activate the NALP3 inflammasome through phagosomal destabilization. Nat Immunol 2008;9:847–56.
[21] Ting JP, Kastner DL, Hoffman HM. CATERPILLERs, pyrin and hereditary immunological disorders. Nat Rev Immunol 2006;6:183–95.
[22] Martinon F, Petrilli V, Mayor A, Tardivel A, Tschopp J. Gout-associated uric acid crystals activate the NALP3 inflammasome. Nature 2006;440:237–41.
[23] Agostini L, Martinon F, Burns K, McDermott MF, Hawkins PN, Tschopp J. NALP3 forms an IL-1beta-processing inflammasome with increased activity in Muckle-Wells autoinflammatory disorder. Immunity 2004;20:319–25.
[24] Mariathasan S, Weiss DS, Newton K, McBride J, O'Rourke K, Roose-Girma M, et al. Cryopyrin activates the inflammasome in response to toxins and ATP. Nature 2006;440:228–32.
[25] Halle A, Hornung V, Petzold GC, Stewart CR, Monks BG, Reinheckel T, et al. The NALP3 inflammasome is involved in the innate immune response to amyloid-beta. Nat Immunol 2008;9:857–65.
[26] Shio MT, Eisenbarth SC, Savaria M, Vinet AF, Bellemare MJ, Harder KW, et al. Malarial hemozoin activates the NLRP3 inflammasome through Lyn and Syk kinases. PLoS Pathog 2009;5:e1000559.
[27] Yoshioka Y, Watanabe H, Morishige T, Yao X, Ikemizu S, Nagao C, et al. Creation of lysine-deficient mutant lymphotoxin-alpha with receptor selectivity by using a phage display system. Biomaterials 2010;31:1935–43.
[28] Busuttil SJ, Ploplis VA, Castellino FJ, Tang L, Eaton JW, Plow EF. A central role for plasminogen in the inflammatory response to biomaterials. J Thromb Haemost 2004;2:1798–805.
[29] Chung EY, Kim SJ, Ma XJ. Regulation of cytokine production during phagocytosis of apoptotic cells. Cell Res 2006;16:154–61.
[30] Fernandes-Alnemri T, Wu J, Yu JW, Datta P, Miller B, Jankowski W, et al. The pyroptosome: a supramolecular assembly of ASC dimers mediating inflammatory cell death via caspase-1 activation. Cell Death Differ 2007;14:1590–604.
[31] Magalhaes AC, Baron GS, Lee KS, Steele-Mortimer O, Dorward D, Prado MA, et al. Uptake and neuritic transport of scrapie prion protein coincident with infection of neuronal cells. J Neurosci 2005;25:5207–16.
[32] Egler RA, Fernandes E, Rothermund K, Sereika S, de Souza-Pinto N, Jaruga P, et al. Regulation of reactive oxygen species, DNA damage, and c-Myc function by peroxiredoxin 1. Oncogene 2005;24:8038–50.
[33] Morel F, Doussiere J, Vignais PV. The superoxide-generating oxidase of phagocytic cells. Physiological, molecular and pathological aspects. Eur J Biochem 1991;201:523–46.
[34] Morishige A, Yoshioka Y, Inakura H, Tanabe A, Yao X, Tsunoda SI, et al. Cytotoxicity of amorphous silica particles against macrophage-like THP-1 cells depends on particle-size and surface properties. Pharmazie in press.
[35] Franchi L, Eigenbrod T, Munoz-Planillo R, Nunez G. The inflammasome: a caspase-1-activation platform that regulates immune responses and disease pathogenesis. Nat Immunol 2009;10:241–7.
[36] Piguet PF, Vesin C, Grau GE, Thompson RC. Interleukin 1 receptor antagonist (IL-1ra) prevents or cures pulmonary fibrosis elicited in mice by bleomycin or silica. Cytokine 1993;5:57–61.
[37] Hawkins PN, Lachmann HJ, McDermott MF. Interleukin-1-receptor antagonist in the Muckle-Wells syndrome. N Engl J Med 2003;348:2583–4.
[38] Kurz T, Terman A, Gustafsson B, Brunk UT. Lysosomes and oxidative stress in aging and apoptosis. Biochim Biophys Acta 2008;1780:1291–303.
[39] Allison AC, Harington JS, Birbeck M. An examination of the cytotoxic effects of silica on macrophages. J Exp Med 1966;124:141–54.
[40] Nadler S, Goldfischer S. The intracellular release of lysosomal contents in macrophages that have ingested silica. J Histochem Cytochem 1970;18:368–71.
[41] Erdogdu G, Hasirci V. An overview of the role of mineral solubility in silicosis and asbestosis. Environ Res 1998;78:38–42.
[42] Ng G, Sharma K, Ward SM, Desrosiers MD, Stephens LA, Schoel WM, et al. Receptor-independent, direct membrane binding leads to cell-surface lipid sorting and Syk kinase activation in dendritic cells. Immunity 2008;29:807–18.
[43] Kuijk LM, Beekman JM, Koster J, Waterham HR, Frenkel J, Coffer PJ. HMG-CoA reductase inhibition induces IL-1beta release through Rac1/PI3K/PKB-dependent caspase-1 activation. Blood 2008;112:3563–73.
[44] Nash T, Allison AC, Harington JS. Physico-chemical properties of silica in relation to its toxicity. Nature 1966;210:259–61.
[45] Pandurangi RS, Seehra MS, Razzaboni BL, Bolsaitis P. Surface and bulk infrared modes of crystalline and amorphous silica particles: a study of the relation of surface structure to cytotoxicity of respirable silica. Environ Health Perspect 1990;86:327–36.
[46] Willingham SB, Bergstralh DT, O'Connor W, Morrison AC, Taxman DJ, Duncan JA, et al. Microbial pathogen-induced necrotic cell death mediated by the inflammasome components CIAS1/cryopyrin/NLRP3 and ASC. Cell Host Microbe 2007;2:147–59.
[47] Fujisawa A, Kambe N, Saito M, Nishikomori R, Tanizaki H, Kanazawa N, et al. Disease-associated mutations in CIAS1 induce cathepsin B-dependent rapid cell death of human THP-1 monocytic cells. Blood 2007;109:2903–11.
[48] Ting JP, Willingham SB, Bergstralh DT. NLRs at the intersection of cell death and immunity. Nat Rev Immunol 2008;8:372–9.

Laboratory of Biotechnology and Therapeutics[1], Graduate School of Pharmaceutical Sciences; The Center for Advanced Medical Engineering and Informatics[2], Osaka University; Laboratory of Pharmaceutical Proteomics[3], National Institute of Biomedical Innovation, Laboratory of Toxicology and Safety Science[4], Graduate School of Pharmaceutical Sciences, Osaka University, Osaka, Japan

Cytotoxicity of amorphous silica particles against macrophage-like THP-1 cells depends on particle-size and surface properties

T. MORISHIGE[1,*], Y. YOSHIOKA[1,2,*], H. INAKURA[1], A. TANABE[1], X. YAO[1], S. TSUNODA[2,3], Y. TSUTSUMI[2,3,4], Y. MUKAI[1], N. OKADA[1], S. NAKAGAWA[1,2]

Received December 17, 2009, accepted January 4, 2010

Yasuo Yoshioka, Ph.D., The Center for Advanced Medical Engineering and Informatics, Osaka University, 1-6 Yamadaoka, Suita, Osaka 565-0871, Japan
yasuo@phs.osaka-u.ac.jp
* Each author contributed equally to the work.

Pharmazie 65: 1–4 (2010) *doi: 10.1691/ph.2010.9408*

Recent studies have indicated that amorphous silica particles (SPs) show cytotoxicity against various types of cells, including macrophages. However, the mechanism of cell death has not been determined, and systematic investigations of the relationship between particle characteristics and cytotoxicity are still quite limited. Here, we compared the cytotoxicity of SPs of various sizes (30–1000 nm) and surface properties against differentiated THP-1 human macrophage-like cells. We found that 300 and 1000 nm SPs showed cytotoxicity against THP-1 cells, whereas 30, 50, and 70 nm SPs did not induce cell death. We demonstrated that 1000 nm SP showed strong cytotoxicity that depended on reactive oxygen species but was independent of caspases. Furthermore, we showed that surface modification of 1000 nm SPs dramatically suppressed their cytotoxicity. Our results suggest that systematic evaluation of the association between particle characteristics and biological effects is necessary for the creation of safe SPs.

1. Introduction

Amorphous (noncrystalline) silica particles (SPs) possess useful properties, including straightforward synthesis, relatively low cost, easy separation, high hydrophilicity, and facile surface modification. In addition, SPs are usually considered to have low toxicity, in contrast to crystalline silica, which can cause silicosis and some forms of lung cancer (Mossman and Churg 1998; Huaux 2007). Therefore, SPs have been used for many applications, including cosmetics, foods, medical diagnosis, cancer therapy, and drug delivery (Hirsch et al. 2003; Bharali et al. 2005; Roy et al. 2005; Bottini et al. 2007; Verraedt et al. 2009).

However, the increasing use of SPs has raised public concern about their safety. In fact, recent studies have found that SPs induce substantial lung inflammation and are cytotoxic against various cells, including macrophages (Wiethoff et al. 2003; Cho et al. 2007; Napierska et al. 2009). Thus, the safety and overall biological effects of SPs have been questioned (Akerman et al. 2002; Kirchner et al. 2005; Dostert et al. 2008). In addition, it has recently become evident that particle characteristics, including particle size and surface properties, are important factors in pathologic alterations and cellular responses (Albrecht et al. 2004; He et al. 2008; Waters et al. 2009). Therefore, investigation of the mechanisms of SP-induced inflammation and cytotoxicity and of the relationship between particle characteristics and cytotoxicity is important for the development of safe SPs.

Here we demonstrate that SPs exhibit cytotoxicity against THP-1 human macrophage-like cells in a size-dependent man-

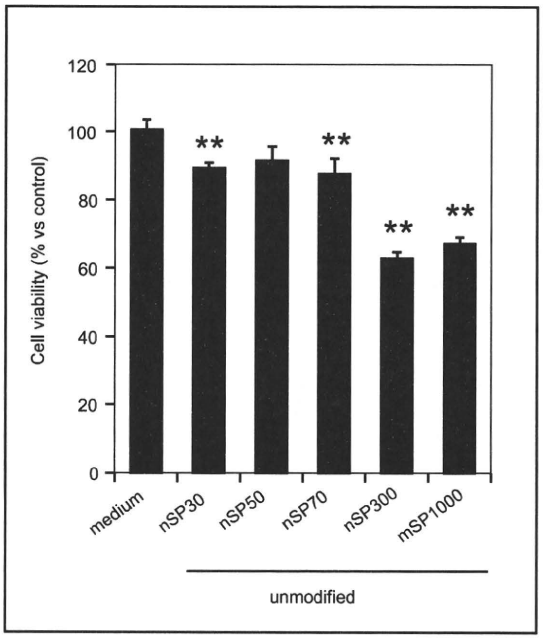

Fig. 1: Correlation between SP particle size and cytotoxicity against macrophage-like cells. PMA-primed THP-1 cells were treated with 100 μg/mL unmodified SPs for 24 h, and cell viability was evaluated by means of the standard methylene blue assay. The data represent the mean ± SD ($n = 5$; $^{**}P < 0.01$ versus value for medium control)

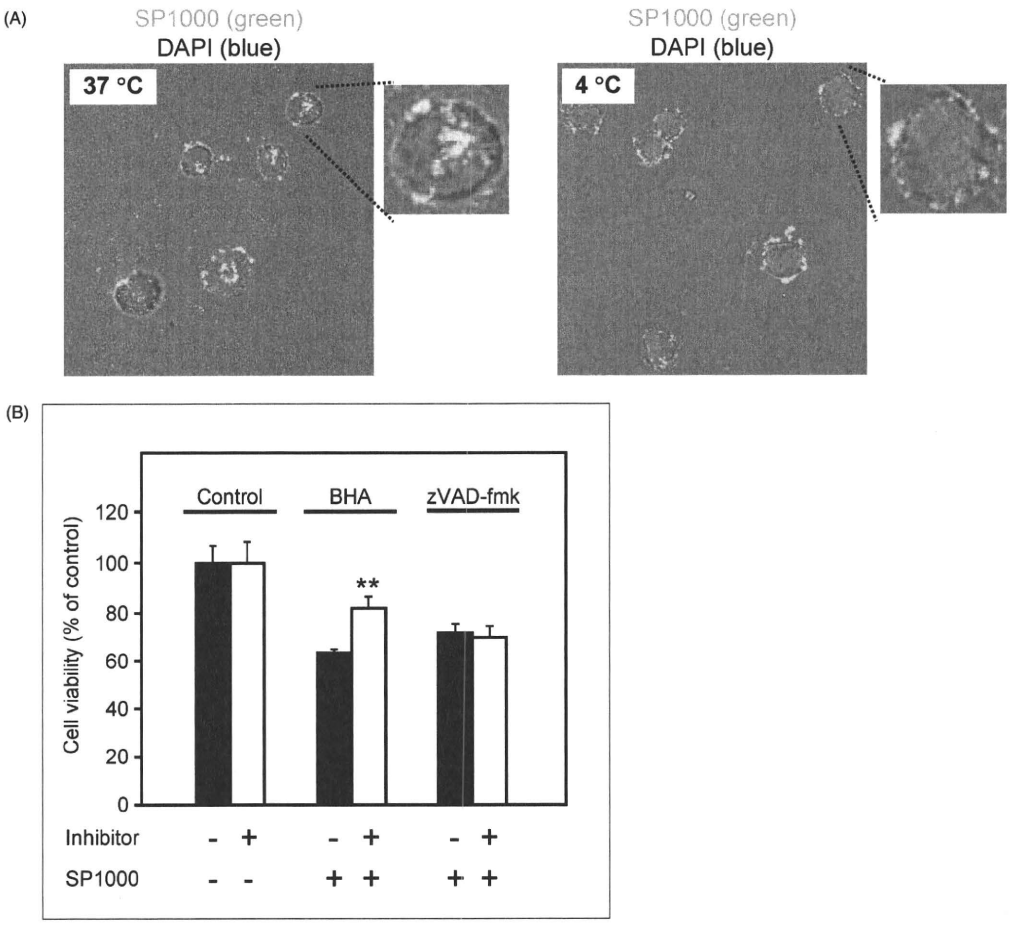

Fig. 2: ROS and caspase dependence of mSP1000-induced cell death. (A) Confocal microscopy images of the ingestion of mSP1000. FITC-conjugated mSP1000 (green) were added to the PMA-primed THP-1 cells at 100 μg/mL. Cells were incubated for 6 h at 37 °C (left) or 4 °C (right). The nucleus was stained with DAPI (blue). (B) Effect of a caspase inhibitor and an ROS scavenger on cytotoxicity of mSP1000. PMA-primed THP-1 cells were treated with 100 (g/mL SP1000s for 24 h in the presence or absence of BHA (150 μM) or zVAD-fmk (60 μM). Cell viability was measured by means of the methylene blue assay. The data represent the mean ± SD ($n = 4$; $^{**}P < 0.01$ versus value for inhibitor [-] control)

ner. Furthermore, we show that SPs with diameters of 1000 nm induce the production of reactive oxygen species (ROS), which triggers THP-1 cell death. We also demonstrate that surface modification of SPs with various functional groups significantly suppresses SP cytotoxicity.

2. Investigations, results and discussion

In this study, we examined whether the size and surface characteristics of SPs are correlated with their cytotoxicity. We also investigated the mechanism by which SPs induce the death of macrophage-like THP-1 cells, with the goal of providing information for the creation of novel safe SPs.

2.1. Amorphous silica particles induce cell death in a size-dependent manner

We used five SPs with diameters between 30 and 1000 nm (nSP30, nSP50, nSP70, nSP300, and mSP1000); the mean secondary particle diameters of the SPs measured by means of a Zetasizer were 33, 44, 79, 326, and 945 nm, respectively (data not shown). To compare the cytotoxicities of the SPs with different diameters, we examined their cytotoxicity against macrophages, which are the first line of defense against infection or injury from various inhaled agents. We incubated phorbol 12-myristate 13-acetate (PMA)-primed human macrophage-like THP-1 cells with SPs and analyzed the levels of cell viability. Twenty-four hours after the incubation, we found that nSP300 and mSP1000 induced marked cytotoxicity, whereas nSP30, nSP50, and nSP70 showed no cytotoxicity (Fig. 1). These results indicate that the particle size of the SPs was intimately involved in their biological effects.

2.2. mSP1000-induced cytotoxicity depends on ROS but not on caspases

Macrophages remove inhaled agents including foreign particles by means of their phagocytic activity. To confirm that THP-1 cells took up mSP1000, we treated THP-1 cells with fluorescein-5-isothiocyanate (FITC)-conjugated mSP1000 at 37 °C or 4 °C. We visually confirmed that mSP1000 were ingested into THP-1 cells at 37 °C, whereas only adsorption of mSP1000 on the cellular surface was detected at 4 °C (Fig. 2A). These results

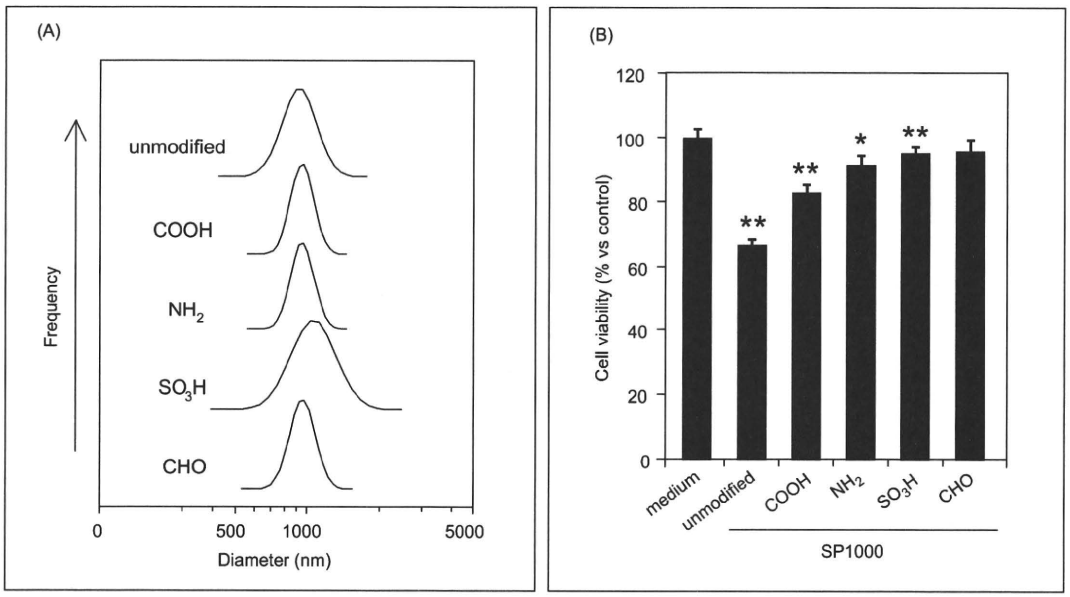

Fig. 3: Correlation between surface modification of mSP1000s and cytotoxicity against macrophage-like THP-1 cells. (A) Particle size distributions of unmodified and surface-modified mSP1000s. Particle size distributions were measured with a Zetasizer 3000HS after sonication at a particle concentration of 300 (g/mL in H_2O. (B) Cytotoxicity of surface-modified mSP1000s. PMA-primed THP-1 cells were treated with the surface-modified mSP1000s at 100 μg/mL for 24 h. After the stimulation, cell viability was measured by means of the standard methylene blue assay. The data represent the mean ± SD ($n = 5$; $^{**}P < 0.01$, $^{*}P < 0.05$ versus value for medium control)

indicate that mSP1000 were recognized and taken up into THP-1 cells by energy-dependent phagocytosis.

We next examined the mechanism of mSP1000-induced cytotoxicity. To determine whether there was an association between caspases and mSP1000-induced cell death, we treated cells with mSP1000 in the presence or absence of zVAD-fmk, a broad caspase inhibitor (it inhibits caspase-1, -3, -4, and -7). We found that zVAD-fmk did not affect the mSP1000-induced cytotoxicity, which indicates that the cytotoxicity was independent of caspases (Fig. 2B). Recently, four kinds of cell death pathways were reported: apoptosis, necrosis, pyroptosis, and pyronecrosis (Ting et al. 2008). Apoptosis and pyroptosis are dependent on the activity of caspases, whereas necrosis and pyronecrosis are independent of caspases. Therefore, our results suggest that mSP1000-induced cell death might have been necrosis or pyronecrosis. Both pathways elicit substantial inflammation, whereas apoptosis is a non-inflammatory cell death that does not affect the area around the dying cells (Ting et al. 2008). Therefore, we suspected that SP-induced cell death might be associated with inflammatory responses induced by mSP1000. However, the stimulation of macrophages with materials such as silica is known to induce ROS production (Msiska et al. 2009). Excessive production of ROS itself causes irreversible cellular injuries and contributes to the pathogenesis of several inflammatory diseases (Cross et al. 1994; Terman et al. 2006). To determine whether ROS were involved in mSP1000-induced cell death, we stimulated THP-1 cells with mSP1000 in the presence of a broad ROS scavenger, butylated hydroxyanisole (BHA), and found that the scavenger significantly inhibited the cytotoxicity of mSP1000 (Fig. 2B). These results indicate that ROS played an important role in the mSP1000-induced cell death and that the cytotoxicity induced by mSP1000 depends on ROS production but is independent of caspases, which suggests that mSP1000-induced cell death is inflammatory necrosis or pyronecrosis.

2.3. mSP1000-induced cell death is suppressed by surface modification with functional groups

To assess the correlation between surface modification and SP cytotoxicity, we used mSP1000 modified with various surface functional groups (-COOH, $-NH_2$, $-SO_3H$, and -CHO). The mean secondary particle diameters of unmodified mSP1000 was 945 nm, and the corresponding values for the modified particles were 1022, 958, 1023, and 969 nm, respectively (Fig. 3A). We compared the cytotoxicity of the modified and unmodified particles against THP-1 cells and found that mSP1000-induced cytotoxicity was suppressed by the surface modification (Fig. 3B). Interestingly, we confirmed that all the surface-modified mSP1000 were taken up equally into the cells (data not shown). We expect that surface modification can be used as a novel method to create safe SPs.

In summary, we confirmed that the cytotoxicity of SPs depended on particle size and surface properties. We confirmed that mSP1000-induced cell death was dependent on ROS production but independent of caspases. We believe that this information will be useful for the creation of novel safe SP-based materials.

3. Experimental

3.1. Materials and reagents

We used SPs with diameters between 30 and 1000 nm (nSP30, nSP50, nSP70, nSP300, and mSP1000), and mSP1000s with various surface functional groups (-COOH, $-NH_2$, $-SO_3H$, and -CHO). The SPs (Sicaster) were purchased from Micromod Partikeltechnologie (Rostock/Warnemünde, Germany). PMA and BHA were purchased from Sigma (St. Louis, MO). zVAD-fmk was purchased from Merck Calbiochem (Darmstadt, Germany).

3.2. Cell treatment

THP-1 cells (human acute monocytic leukemia cell line) were obtained from the American Type Culture Collection (Manassas, VA) and were cultured in RPMI-1640 (Wako Pure Chemical Industries, Osaka, Japan) supplemented

with 10% fetal bovine serum, 2 mM L-glutamine, and antibiotics at 37 °C. Treatment of THP-1 cells with PMA reportedly induces differentiation to a macrophage phenotype (Hoff et al. 1992; Rutault et al. 2001).

3.3. *Size distribution of silica particles*

The size distributions of the SP were measured with a Zetasizer 3000HS (Malvern, Worcestershire, UK) after sonication at a particle concentration of 300 μg/mL in H_2O.

3.4. *Cytotoxicity of various silica particles*

THP-1 cells (1.5×10^4 cells/well) were seeded in 96-well plates, differentiated to macrophages by incubation with 0.5 (M PMA for 24 h, and then washed once with incubation medium. After the PMA priming, cells were treated with 100 (g/mL SPs for 24 h. The cytotoxicity of the SPs against THP-1 cells was assessed by means of the standard methylene blue assay. In brief, after the SP treatment, cells were fixed with 100 μL of 2.5% glutaraldehyde for 15 min and stained with 100 μL of 0.05% methylene blue for 15 min. Then, the cells were lysed with 200 μL of 0.33 N HCl. The $OD_{655-415}$ was measured using a multiwell spectrophotometer (Molecular Devices, Inc., Tokyo, Japan).
For the inhibitory assays, PMA-primed THP-1 cells were pre-incubated with BHA (150 μM) or zVAD-fmk (60 μM) for 30 min and then treated with 100 μg/mL SPs for 24 h in the presence or absence of each inhibitor.

3.5. *Laser scanning confocal microscopy analysis*

THP-1 cells (1.0×10^5 cells/well) were seeded on Lab-Tek II Chambered Coverglass (Nunc, Rochester, NY), differentiated to macrophages by incubation with 0.5 μM PMA for 24 h, and treated for 6 h with 100 μg/mL mSP1000s. Then the cells were washed and fixed with 4% paraformaldehyde and mounted with Prolong Gold with 2-(4-amidinophenyl)-1*H*-indole-6-carboxamidine (DAPI, Invitrogen, Carlsbad, CA) for nuclear staining. Fluorescence was observed with a laser scanning confocal microscope (Leica Microsystems GmbH, Wetzlar, Germany).

3.6. *Statistical analysis*

All results are presented as means ± standard deviation (SD). Differences were compared using Student's *t*-test or Scheffé's method after analysis of variance (ANOVA).

Acknowledgements: The authors declare that they have no conflicts of interest. This study was supported in part by grants from the Ministry of Health, Labor, and Welfare in Japan.

References

Akerman ME, Chan WC, Laakkonen P, Bhatia SN, Ruoslahti E (2002) Nanocrystal targeting *in vivo*. Proc Natl Acad Sci U S A 99: 12617–12621.

Albrecht C, Schins RP, Hohr D, Becker A, Shi T, Knaapen AM, Borm PJ (2004) Inflammatory time course after quartz instillation: role of tumor necrosis factor-alpha and particle surface. Am J Respir Cell Mol Biol 31: 292–301.

Bharali DJ, Klejbor I, Stachowiak EK, Dutta P, Roy I, Kaur N, Bergey EJ, Prasad PN, Stachowiak MK (2005) Organically modified silica nanoparticles: a nonviral vector for *in vivo* gene delivery and expression in the brain. Proc Natl Acad Sci U S A 102: 11539–11544.

Bottini M, D'Annibale F, Magrini A, Cerignoli F, Arimura Y, Dawson MI, Bergamaschi E, Rosato N, Bergamaschi A, Mustelin T (2007) Quantum dot-doped silica nanoparticles as probes for targeting of T-lymphocytes. Int J Nanomedicine 2: 227–233.

Cho WS, Choi M, Han BS, Cho M, Oh J, Park K, Kim SJ, Kim SH, Jeong J (2007) Inflammatory mediators induced by intratracheal instillation of ultrafine amorphous silica particles. Toxicol Lett 175: 24–33.

Cross CE, van der Vliet A, O'Neill CA, Eiserich JP (1994) Reactive oxygen species and the lung. Lancet 344: 930–933.

Dostert C, Petrilli V, Van Bruggen R, Steele C, Mossman BT, Tschopp J (2008) Innate immune activation through Nalp3 inflammasome sensing of asbestos and silica. Science 320: 674–677.

He X, Nie H, Wang K, Tan W, Wu X, Zhang P (2008) *In vivo* study of biodistribution and urinary excretion of surface-modified silica nanoparticles. Anal Chem 80: 9597–9603.

Hirsch LR, Stafford RJ, Bankson JA, Sershen SR, Rivera B, Price RE, Hazle JD, Halas NJ, West JL (2003) Nanoshell-mediated near-infrared thermal therapy of tumors under magnetic resonance guidance. Proc Natl Acad Sci U S A 100: 13549–13554.

Hoff T, Spencker T, Emmendoerffer A, Goppelt-Struebe M (1992) Effects of glucocorticoids on the TPA-induced monocytic differentiation. J Leukoc Biol 52: 173–182.

Huaux F (2007) New developments in the understanding of immunology in silicosis. Curr Opin Allergy Clin Immunol 7: 168–173.

Kirchner C, Liedl T, Kudera S, Pellegrino T, Munoz Javier A, Gaub HE, Stolzle S, Fertig N, Parak WJ (2005) Cytotoxicity of colloidal CdSe and CdSe/ZnS nanoparticles. Nano Lett 5: 331–338.

Mossman BT, Churg A (1998) Mechanisms in the pathogenesis of asbestosis and silicosis. Am J Respir Crit Care Med 157: 1666–1680.

Msiska Z, Pacurari M, Mishra A, Leonard SS, Castranova V, Vallyathan V (2009) DNA double strand breaks by asbestos, silica and titanium dioxide: possible biomarker of carcinogenic potential? Am J Respir Cell Mol Biol in print.

Napierska D, Thomassen LC, Rabolli V, Lison D, Gonzalez L, Kirsch-Volders M, Martens JA, Hoet PH (2009) Size-dependent cytotoxicity of monodisperse silica nanoparticles in human endothelial cells. Small 5: 846–853.

Roy I, Ohulchanskyy TY, Bharali DJ, Pudavar HE, Mistretta RA, Kaur N, Prasad PN (2005) Optical tracking of organically modified silica nanoparticles as DNA carriers: a nonviral, nanomedicine approach for gene delivery. Proc Natl Acad Sci U S A 102: 279–284.

Rutault K, Hazzalin CA, Mahadevan LC (2001) Combinations of ERK and p38 MAPK inhibitors ablate tumor necrosis factor-alpha (TNF-alpha) mRNA induction. Evidence for selective destabilization of TNF-alpha transcripts. J Biol Chem 276: 6666–6674.

Terman A, Gustafsson B, Brunk UT (2006) The lysosomal-mitochondrial axis theory of postmitotic aging and cell death. Chem Biol Interact 163: 29–37.

Ting JP, Willingham SB, Bergstralh DT (2008) NLRs at the intersection of cell death and immunity. Nat Rev Immunol 8: 372–379.

Verraedt E, Pendela M, Adams E, Hoogmartens J, Martens JA (2009) Controlled release of chlorhexidine from amorphous microporous silica. J Control Release.

Waters KM, Masiello LM, Zangar RC, Tarasevich BJ, Karin NJ, Quesenberry RD, Bandyopadhyay S, Teeguarden JG, Pounds JG, Thrall BD (2009) Macrophage responses to silica nanoparticles are highly conserved across particle sizes. Toxicol Sci 107: 553–569.

Wiethoff AJ, Reed KL, Webb TR, Warheit DB (2003) Assessing the role of neutrophil apoptosis in the resolution of particle-induced pulmonary inflammation. Inhal Toxicol 15: 1231–1246.

Biomaterials 32 (2011) 3–9

Contents lists available at ScienceDirect

Biomaterials

journal homepage: www.elsevier.com/locate/biomaterials

Leading Opinion

Acute phase proteins as biomarkers for predicting the exposure and toxicity of nanomaterials☆

Kazuma Higashisaka [a,b,1], Yasuo Yoshioka [a,b,c,*,1], Kohei Yamashita [a,b], Yuki Morishita [a,b], Maho Fujimura [a,b], Hiromi Nabeshi [a], Kazuya Nagano [b], Yasuhiro Abe [b], Haruhiko Kamada [b,c], Shin-ichi Tsunoda [b,c,d], Tomoaki Yoshikawa [a,b], Norio Itoh [a], Yasuo Tsutsumi [a,b,c,**]

[a] Department of Toxicology and Safety Science, Graduate School of Pharmaceutical Sciences, Osaka University, 1-6 Yamadaoka, Suita, Osaka 565-0871, Japan
[b] Laboratory of Pharmaceutical Proteomics, National Institute of Biomedical Innovation, 7-6-8, Saito-Asagi, Ibaraki, Osaka 567-0085, Japan
[c] The Center for Advanced Medical Engineering and Informatics, Osaka University, 1-6, Yamadaoka, Suita, Osaka 565-0871, Japan
[d] Department of Biomedical Innovation, Graduate School of Pharmaceutical Sciences, Osaka University, 7-6-8, Saito-Asagi, Ibaraki, Osaka 567-0085, Japan

ARTICLE INFO

Article history:
Received 8 July 2010
Accepted 31 August 2010
Available online 22 September 2010

Keywords:
Nanoparticle
Plasma proteins
Silica
Surface modification

ABSTRACT

Recently, nanomaterials have become an integral part of our daily lives. However, there is increasing concern about the potential risk to human health. Here, we attempted to identify biomarkers for predicting the exposure and toxicity of nanomaterials by using a proteomics based approach. We evaluated the changes of protein expression in plasma after treatment with silica nanoparticles. Our analyses identified haptoglobin, one of the acute phase proteins, as a candidate biomarker. The results of ELISA showed that the level of haptoglobin was significantly elevated in plasma of mice exposed to silica nanoparticles with a diameter of 70 nm (nSP70) compared to normal mice and those exposed to silica particles with a diameter of 1000 nm. Furthermore, the other acute phase proteins, C-reactive protein (CRP) and serum amyloid A (SAA) were also elevated in plasma of nSP70 treated mice. In addition, the level of these acute phase proteins was elevated in the plasma of mice after intranasal treatment with nSP30. Our results suggest that haptoglobin, CRP and SAA are highly sensitive biomarkers for assessing the risk of exposure to silica nanoparticles. We believe this study will contribute to the development of global risk assessment techniques for nanomaterials.

1. Introduction

With the recent development of nanotechnology, nanomaterials such as silica nanoparticles are beginning to be used on a global scale. In comparison to conventional materials with submicron size, nanomaterials display unique properties such as high levels of electrical conductivity, tensile strength and chemical reactivity [1]. Nanomaterials have already been used in various fields such as electronic engineering, cosmetics and medicine [2,3]. Because nanotechnology is emerging as a leading industrial sector, humans will be increasingly exposed to a wide range of synthetic nanomaterials with diverse properties.

The increasing use of nanomaterials has raised public concerns about the potential risks to human health [4–6]. For example, it is reported that carbon nanotubes induce mesothelioma-like lesions in mice in a similar way to crocidolite asbestos [7]. Other reports showed that exposure to titanium dioxide particles induce inflammatory responses and lung injury in mice [8,9]. In addition, our group showed that silica nanoparticles with a diameter of 70 nm can penetrate mouse skin and enter the circulatory system (unpublished data). Furthermore our group demonstrated that silica nanoparticles induce severe liver damage after systemic administration [10–12]. However, current knowledge of the potential risk of nanomaterials is considered insufficient. Indeed, concerns about the potential dangers of nanomaterials have led the World Health Organization and the Organization for Economic

☆ *Editor's Note*: This paper is one of a newly instituted series of scientific articles that provide evidence-based scientific opinions on topical and important issues in biomaterials science. They have some features of an invited editorial but are based on scientific facts, and some features of a review paper, without attempting to be comprehensive. These papers have been commissioned by the Editor-in-Chief and reviewed for factual, scientific content by referees.

* Corresponding author. The Center for Advanced Medical Engineering and Informatics, Osaka University, 1-6 Yamadaoka, Suita, Osaka 565-0871, Japan. Tel.: +81 6 6879 8230; fax: +81 6 6879 8234.

** Corresponding author. Department of Toxicology and Safety Science, Graduate School of Pharmaceutical Sciences, Osaka University, 1-6, Yamadaoka, Suita, Osaka 565-0871, Japan. Tel.: +81 6 6879 8230; fax: +81 6 6879 8234.

E-mail addresses: yasuo@phs.osaka-u.ac.jp (Y. Yoshioka), ytsutsumi@phs.osaka-u.ac.jp (Y. Tsutsumi).

[1] These authors contributed equally to the work.

0142-9612/$ – see front matter © 2010 Elsevier Ltd. All rights reserved.
doi:10.1016/j.biomaterials.2010.08.110

Co-operation and Development to call for an urgent and detailed evaluation of their safety. Therefore, it is extremely important to progress these safety evaluations in order to facilitate the development of nanomaterials that are harmless to humans, because nanomaterials have the potential to improve the quality of human life. In particular, it is hoped that a risk assessment system can be developed to estimate or predict the safety and toxicity of nanomaterials.

Molecular biomarkers, obtained from biological samples such as blood, urine and tissue, constitute an objective indicator for correlating against various physiological conditions or variation of disease state [13,14]. By using biomarkers, we are able to predict not only the present disease and clinical condition but the risk of acquiring disease in the future. Nowadays, biomarkers that act as predictors of cancer have already been developed and are commonly used in clinical practice [14]. Furthermore, such an approach is capable of predicting adverse effects of drugs and medicines [15,16]. By contrast, studies of biomarkers for nanomaterials have barely advanced. These biomarkers would represent the unity of local and systemic physiological responses induced as a result of the exposure. Therefore, biomarkers for nanomaterials will be invaluable for predicting their potential toxicity and establishing strategies for the safe development of nanomaterials production and use.

Here we attempted to develop potential biomarkers of nanomaterials using a proteomics analysis with the aim of developing safe forms of nanomaterials.

2. Materials and methods

2.1. Materials

Silica particles were purchased from *Micromod* Partikeltechnologie (Rostock/Warnemünde, Germany). The silica particles with diameters of 30, 70, 300 and 1000 nm (nSP30, nSP70, nSP300 and mSP1000, respectively), and nSP70 with surface functional groups such as carboxyl group and amino group (nSP70-C and nSP70-N, respectively) were used in this study. The silica particles were sonicated for 5 min and vortexed for 1 min prior to use.

2.2. Animals

Female BALB/c mice were purchased from Nippon SLC, Inc (Shizuoka, Japan) and used at 6–8 weeks of age. All of the animal experimental procedures in this study were performed in accordance with the National Institute of Biomedical Innovation guidelines for the welfare of animals.

2.3. Blood sample collection

For administration of silica particles through an intravenous route, BALB/c mice were treated with nSP70, nSP300, mSP1000, nSP70-C, nSP70-N or saline at 0.8 mg/mouse. At various times (6 h, 24 h, 3 day and 7 day) after treatment of these silica particles, blood samples were collected. For administration of silica particles through an intranasal route, BALB/c mice were treated with nSP30, nSP70 or saline intranasally at 0.5 mg/mouse. Blood samples were collected 24 h after the treatment of these silica nanoparticles.

2.4. Analysis of biomarkers for nanomaterials using a proteomics approach

BALB/c mice were treated with 0.8 mg/mouse nSP70 or saline intravenously. After 24 h, blood samples were collected and plasma was harvested by centrifuging blood at 12000 rpm for 15 min. Proteo prep (Sigma–Aldrich; Saint Louis, MO) was used to remove albumin and immunoglobulins from the plasma according to the manufacturer's instructions. Plasma samples were then analyzed by sodium dodecyl sulfate-polyacrylamide gel electrophoresis (SDS-PAGE) followed by Coomassie Brilliant Blue staining. Plasma diluted into aliquots corresponding to 10 μg protein were mixed with an equal volume of Laemmli sample buffer (BIO-RAD, Tokyo, Japan) containing 5% 2-mercaptethanol and boiled for 5 min prior to electrophoresis. Electrophoresis was performed at 15 mA for 10 min (stacking) followed by separation (600 V, 40 mA, 100 W) for approximately 45 min, using Precision Plus Protein Kaleidoscope molecular weight markers (BIO-RAD) as standards.

2.5. Identification of candidate proteins as biomarkers

Bands of interest were excised from the gel and then destained with 50% acetonitrile (ACN)/25 mM NH_4HCO_3 for 10 min, dehydrated with 100% ACN for 10 min, and then dried using a centrifugal concentrator. Next, 8 μl of 20 μl/ml trypsin solution (Promega, Madison, WI) diluted 5-fold in 50 mM NH_4HCO_3 was added to each gel piece and then incubated overnight at 37 °C. We used three solutions to extract the resulting peptide mixtures from the gel pieces. First, 50 μl of 50% (v/v) ACN in 0.1% aqueous trifluoroacetic acid (TFA) was added to the gel pieces, which were then sonicated for 30 min. Next, we collected the solution and added 80% (v/v) ACN in 0.1% TFA. Finally, 100% ACN was added for the last extraction. The peptide solution were dried and resuspended in 10 μl of 0.1% formic acid. The resulting peptide mixture was then analyzed by nano-flow liquid chromatography/tandem mass spectrometry (LC/MS; maXis, Bruker Daltonik GmbH, Bremen, Germany).

2.6. Measurement of acute phase proteins

Plasma levels of haptoglobin, C-reactive protein (CRP) and serum amyloid A (SAA) were measured by commercial enzyme-linked immunosorbent assay (ELISA) kits (Life Diagnostics, Inc.; West Chester, PA), according to the manufacturer's instructions.

2.7. Statistical analyses

All results are expressed as means ± SD. Differences were compared by using the Bonferroni's method after analysis of variance (ANOVA).

3. Results

3.1. Identification of biomarkers of nanomaterials

We used silica particles as a model nanomaterial because it is one of the most common nanomaterials to have been developed. Silica particles are increasingly being used as additives in cosmetics and foods [17,18]. It is predicted that the global market for silica particles will soon grow to $2 billion and a ton of silica particles is currently produced worldwide every year. Here, we used silica particles with a diameter of 30, 70, 300 and 1000 nm (nSP30, nSP70, nSP300 and mSP1000, respectively). The mean secondary particle diameters of the silica particles measured by Zetasizer were 33, 79, 326 and 945 nm, respectively (data not shown). The silica particles were confirmed to be well dispersed smooth-surfaced spheres by transmission electron microscopy (data not shown).

Initially, we attempted to identify protein biomarkers in mice by analyzing changes in the level of each plasma protein following treatment with silica nanoparticles using a proteomics approach. BALB/c mice were intravenously treated with nSP70 (0.8 mg/mouse) or saline and then plasma samples were collected 24 h later. Because albumin and immunoglobulins are known to account for the majority of plasma proteins, they were removed from the samples prior to analysis so that variation in the level of other proteins could be more closely monitored. The change of protein levels in plasma after treatment with nSP70 was assessed by SDS-PAGE analysis (Fig. 1). The intensity of a band of molecular mass 37 kDa was more intense in the plasma of nSP70 treated mice than that of saline treated control mice (Fig. 1). The band was excised and analyzed by LC/MS in order to identify the corresponding protein. This analysis identified the induced band after treatment with nSP70 as haptoglobin, one of the acute phase proteins.

3.2. The level of haptoglobin after treatment with silica particles

To assess the change of haptoglobin level in plasma after administration of silica particles, BALB/c mice were intravenously treated with nSP70, nSP300 or mSP1000 at 0.8 mg/mouse. We did not use nSP30 in the experiment, because nSP30 induced the toxic side effects after intravenous treatment at this dose. We confirmed that nSP70, nSP300 or mSP1000 at this dose did not induce any

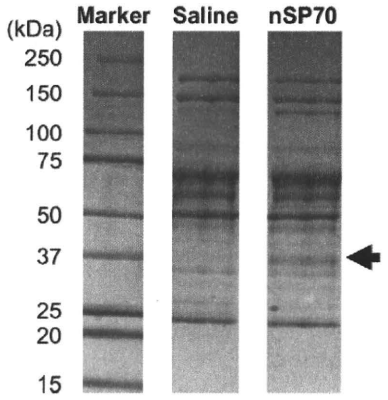

Fig. 1. SDS-PAGE analysis of plasma proteins. BALB/c mice were intravenously treated with nSP70 or saline at 0.8 mg/mouse. After 24 h, blood samples were collected. The change of protein levels in plasma after treatment of nSP70 was assessed by SDS-PAGE.

significant elevation of tissue injury and dysfunction markers such as alanine aminotransferase (ALT), aspartate aminotransferase (AST) and blood urea nitrogen (BUN) (data not shown). After 24 h, the level of haptoglobin in the plasma was analyzed by ELISA (Fig. 2A). The levels of haptoglobin in the plasma of nSP70 treated mice were significantly higher than those of saline treated control mice. In contrast, the levels of haptoglobin in the plasma of mSP1000 treated mice were almost the same as those of the saline treated control group. The haptoglobin levels of nSP300 treated mice were slightly higher than those of saline treated control mice. These results indicate that the levels of haptoglobin in the plasma of mice increase as the silica particle size decreases. Thus, haptoglobin appears to be a valuable biomarker for exposure to silica particles of nanometer size.

To assess the potential of haptoglobin as biomarker more precisely, we examined the sensitivity and time dependency of changes in haptoglobin level after treatment with silica particles. BALB/c mice were treated with nSP70, nSP300 or mSP1000 intravenously at 0.8 mg/mouse. After 6 h, 24 h, 3 day and 7 day, we examined the level of haptoglobin in the plasma by ELISA (Fig. 2B). No elevation of haptoglobin in the plasma of mSP1000 treated mice was observed. However, nSP70 and nSP300 treated mice showed a maximum level of haptoglobin 24 h after treatment. Furthermore, at 3 days after treatment, the level of haptoglobin in nSP70 treated mice was significantly higher than saline treated control mice. Next, BALB/c mice were treated with 0.2 and 0.05 mg/mouse nSP70 intravenously. After 24 h, we examined the level of haptoglobin in the plasma by ELISA (Fig. 2C). Mice treated with 0.2 and 0.05 mg/mouse nSP70 did not show any elevated level of haptoglobin. These results indicate that the level of haptoglobin is elevated as the particle size of silica particles decreases and that an increase of haptoglobin is dependent on the concentration of silica particles.

3.3. Response of other acute phase proteins

Haptoglobin, CRP and SAA are typical acute phase proteins that are induced during infection and inflammation [19]. To assess the levels of CRP and SAA in plasma after administration of silica particles, BALB/c mice were intravenously treated with nSP70, nSP300 or mSP1000 at 0.8 mg/mouse. After 6 h, 24 h, 3 day and 7 day, we examined the level of CRP (Fig. 3A) and SAA (Fig. 3B) in the plasma of the mice by ELISA. At 6 h and 24 h, both the level of CRP and SAA in the plasma of mice treated with nSP70 was significantly higher than those of the saline treated control mice. Furthermore, the maximum level of CRP in nSP70 treated mice was observed at

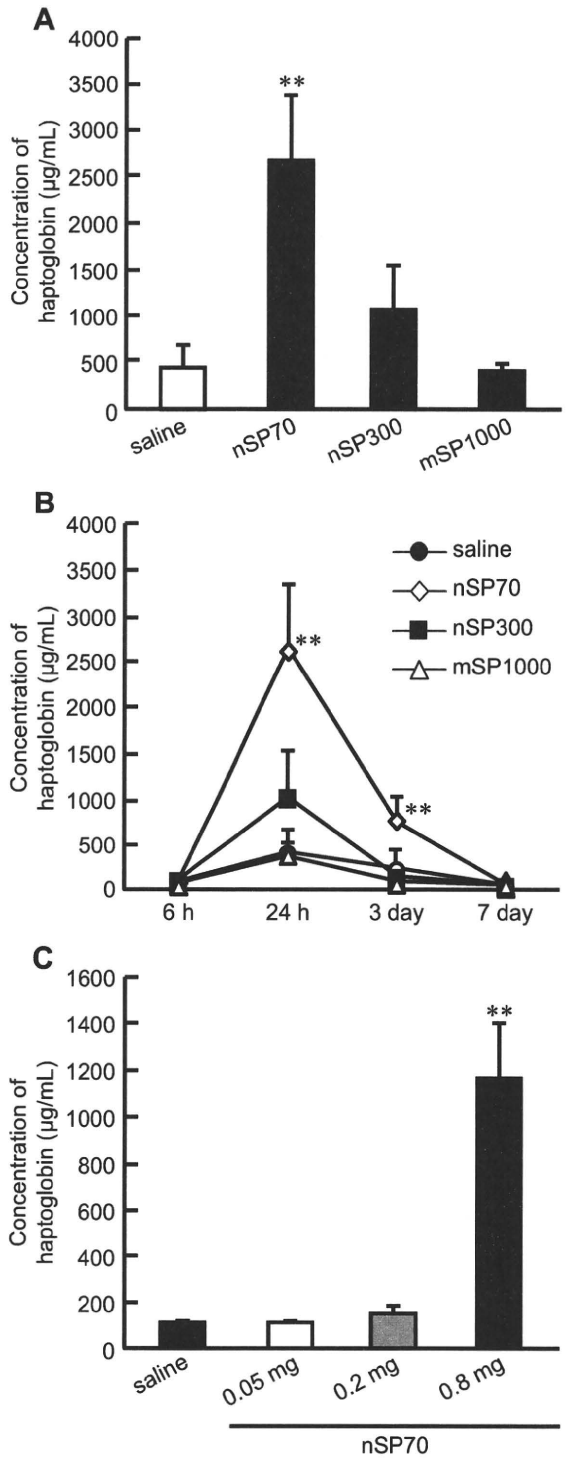

Fig. 2. The potential of haptoglobin as biomarker of nanomaterials. (A) The level of haptoglobin after treatment with silica particles. BALB/c mice were intravenously treated with nSP70, nSP300 or mSP1000 at 0.8 mg/mouse. After 24 h, the level of haptoglobin in the plasma of each mouse was examined by ELISA. (B) The time dependency of haptoglobin expression after treatment with silica particles. BALB/c mice were intravenously treated with nSP70, nSP300 or mSP1000 at 0.8 mg/mouse. After 6 h, 24 h, 3 day and 7 day, blood samples were collected. The level of haptoglobin in the plasma of the mice was determined by ELISA. (C) The sensitivity of haptoglobin after treatment of silica particles. BALB/c mice were intravenously treated with nSP70 at 0.8, 0.2 or 0.05 mg/mouse. After 24 h, blood samples were collected. The level of haptoglobin in the plasma of treated mice was determined by ELISA. Data are presented as mean ± SD ($n = 5$–6; $^{**}P < 0.01$ *versus* value for saline treated group by ANOVA).

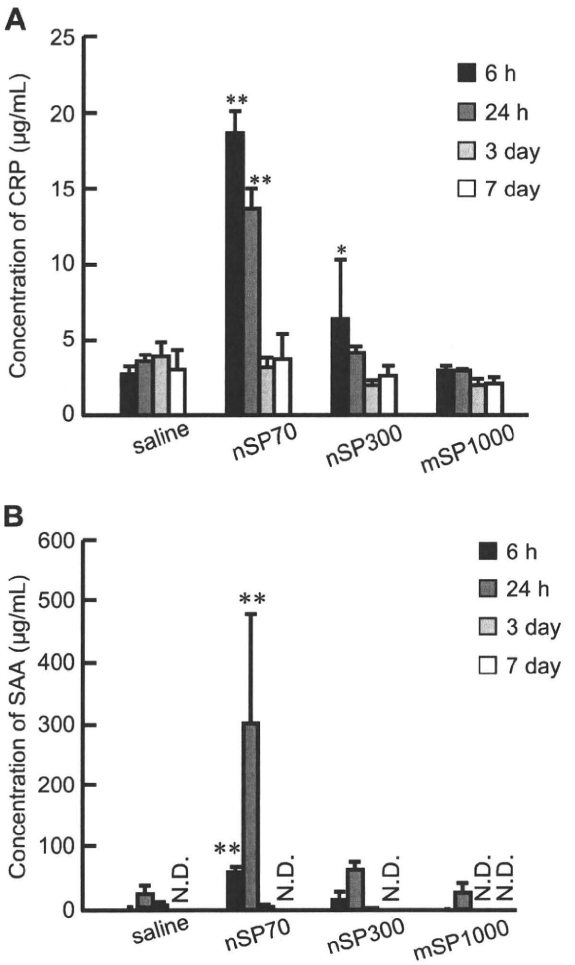

Fig. 3. Response of other acute phase proteins. BALB/c mice were intravenously treated with nSP70, nSP300 or mSP1000 at 0.8 mg/mouse. After 6 h, 24 h, 3 day and 7 day, blood samples were collected. The levels of (A) CRP and (B) SAA in the plasma of treated mice were examined by ELISA. Data are presented as mean ± SD ($n = 5–6$; $*P < 0.05$, $**P < 0.01$ *versus* value for saline treated group by ANOVA; N.D., not detected).

6 h after treatment, whereas that of haptoglobin and SAA was observed at 24 h. In contrast, the level of CRP and SAA in plasma of mSP1000 treated mice were almost the same as that of the saline treated control mice at all time points. The level of CRP in the plasma of nSP300 treated mice was slightly higher than that of saline treated control mice at 6 h. Our results suggest that both SAA and CRP may be useful biomarkers for predicting the risk from exposure to silica nanoparticles as well as haptoglobin. Indeed, these biomarkers could give even better response and sensitivity when used in combination.

3.4. The level of acute phase proteins through various routes

Exposure to nanomaterials in our daily lives can occur through various different routes. For example, nanomaterials contained in foods and drug medicines are taken up orally, whereas nanomaterials spread in the environment generally enter the body intranasally. Therefore, there is a need to evaluate suitable biomarkers for the exposure of nanomaterials through various routes. To assess the response of acute phase proteins to

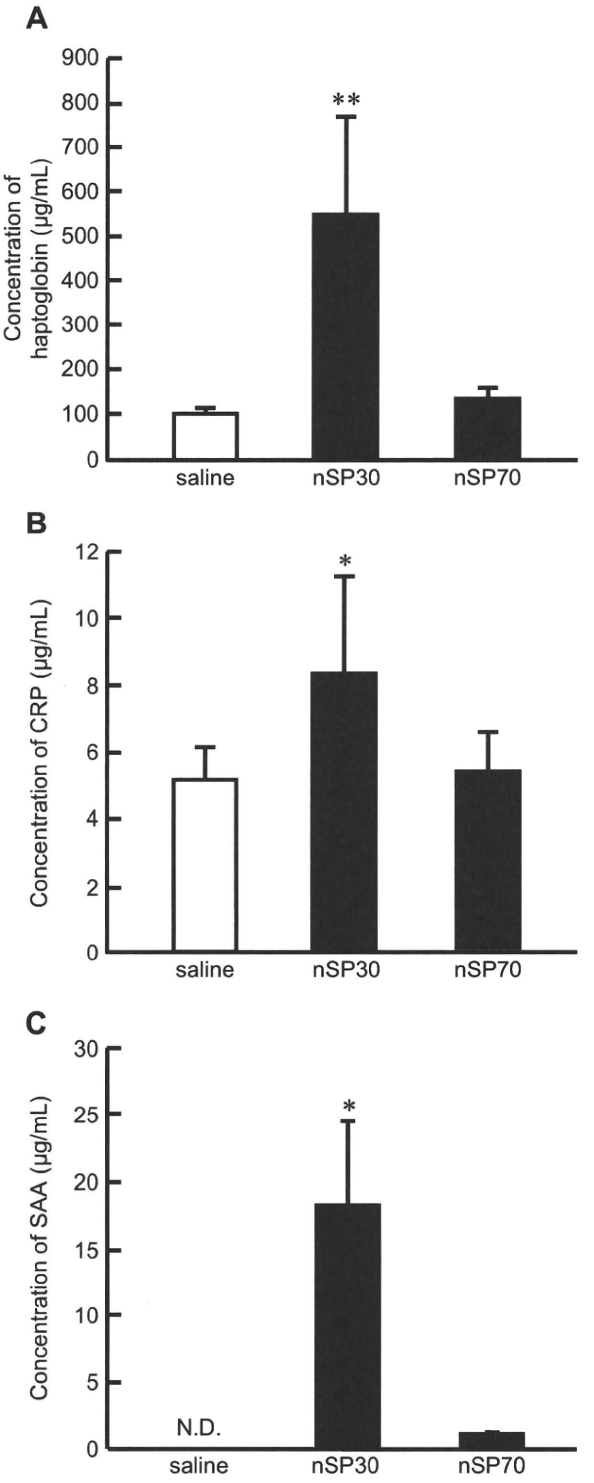

Fig. 4. Application of acute phase proteins to assess exposure of nanomaterials through various routes. To assess the administration of silica nanoparticles through an intranasal route, BALB/c mice were treated with nSP30, nSP70 or saline intranasally at 0.5 mg/mouse. Blood samples were collected 24 h after treatment. The level of (A) haptoglobin, (B) CRP and (C) SAA in the plasma were examined by ELISA. Data are presented as mean ± SD ($n = 5–6$; $*P < 0.05$, $**P < 0.01$ *versus* value for saline treated group by ANOVA; N.D., not detected).

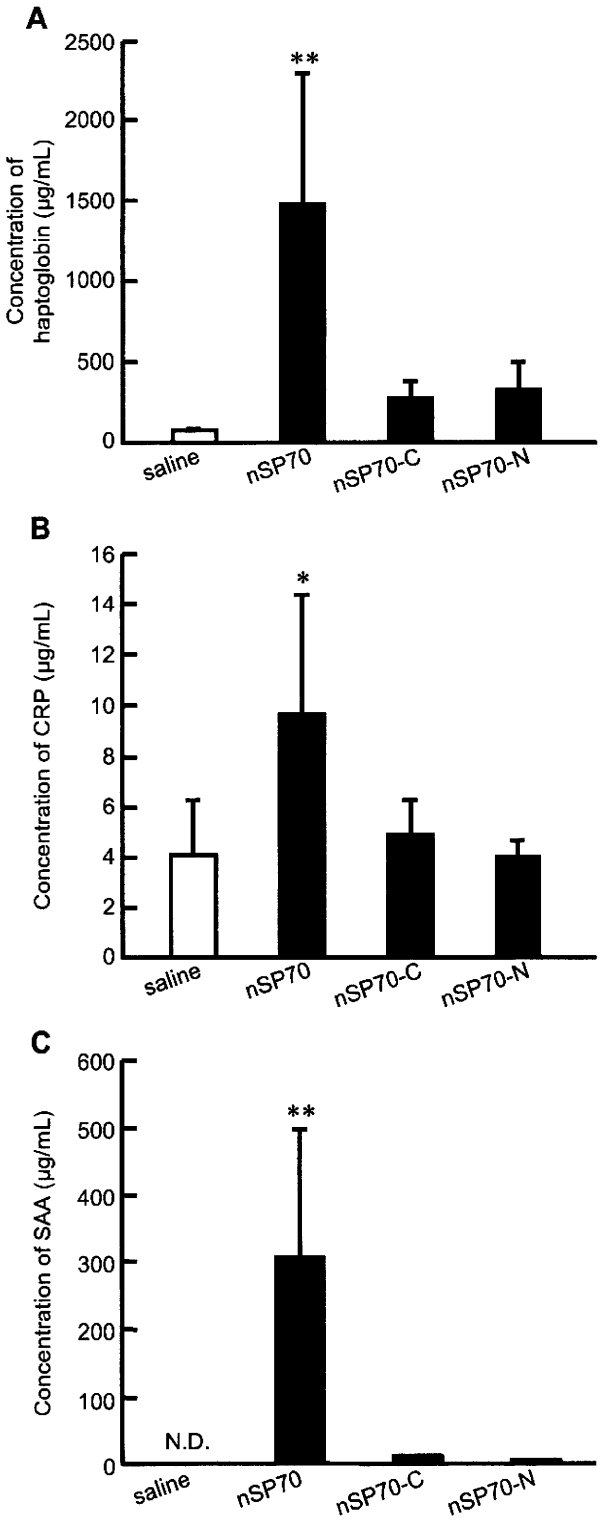

Fig. 5. Responses of acute phase proteins by the exposure to surface modified nSP70. BALB/c mice were intravenously treated with nSP70 modified with amino or carboxyl groups at 0.8 mg/mouse. After 24 h, the level of (A) haptoglobin, (B) CRP and (C) SAA in the plasma of treated mice were examined by ELISA. Data are presented as mean ± SD ($n = 5–6$; $^*P < 0.05$, $^{**}P < 0.01$ *versus* value for saline treated group by ANOVA; N.D., not detected).

silica particles introduced *via* different routes, we examined the level of haptoglobin, CRP and SAA in plasma after treatment of silica particles intranasally (Fig. 4). In this experiment, we used nSP30 and nSP70. For the administration of silica nanoparticles through an intranasal route, BALB/c mice were treated with nSP30, nSP70 or saline intranasally at 0.5 mg/mouse. After 24 h, we examined the level of haptoglobin (Fig. 4A), CRP (Fig. 4B) and SAA (Fig. 4C) in the plasma of the mice by ELISA. We showed that the level of haptoglobin, CRP and SAA in the plasma of mice treated with nSP30 intranasally was significantly higher than those of the saline treated control mice, although intranasal administration of nSP70 did not cause elevation in the plasma level of each acute phase protein in the treated mice. These results suggest that acute phase proteins could be useful biomarkers for predicting the risk arising from exposure to silica nanoparticles through various routes.

3.5. The level of acute phase proteins after treatment with surface modified silica nanoparticles

It has recently become evident that particle characteristics, including particle size and surface properties, are important factors in pathologic alterations and cellular responses [8,20–22]. Previously, our group also showed that surface modification of silica particles with functional groups such as amino or carboxyl group suppressed toxic biological effects of silica particles such as inflammatory responses [23]. To assess whether acute phase proteins could be useful biomarkers to predict risk factors associated with exposure to silica particles, we examined the level of haptoglobin (Fig. 5A), CRP (Fig. 5B) and SAA (Fig. 5C) in the plasma of mice after administration of nSP70 with amino or carboxyl group surface modifications. BALB/c mice were treated with 0.8 mg/mouse of these silica particles intravenously. After 24 h, we examined the level of haptoglobin, CRP and SAA in the plasma of the treated mice by ELISA. Our results showed that the level of these acute phase proteins in the plasma of nSP70 with amino or carboxyl group treated mice were significantly low compared with nSP70 treated mice.

4. Discussion

Our goal was to identify the biomarkers of nanomaterials for predicting their potential toxicity and to provide basic information for the creation of safe nanomaterials. To achieve these purposes, we tried to identify biomarkers in blood using a proteomics analysis. At first, we showed that the silica nanoparticles with small particle sizes (diameter <100 nm) induced a higher level of acute phase proteins such as haptoglobin, CRP and SAA than larger silica particles (diameter >100 nm) after intravenously treatment (Figs. 2 and 3). Previously, our group has shown that silica nanoparticles with relatively small particle size such as nSP70 induce a greater level of toxicity, including liver injury, compared to those of larger particle size [10,11]. Thus, there is a correlation between toxicity induced by the silica nanoparticles and the level of each potential plasma biomarker. Therefore, these acute phase proteins appear to be good biomarkers for predicting the strength of toxicity induced by silica nanoparticles.

The acute phase response is the nonspecific early response of an organism to infection and inflammation[24]. It comprises a whole array of systemic reactions and induction of a group of serum proteins called the acute phase proteins [25]. Monitoring the progression of infection and cancer by acute phase protein measurements in blood samples is used extensively in human patients. For example, haptoglobin is a biomarker of pancreatic cancer [26]. CRP is used as an index for the development of atrial fibrillation and maintenance [27], although mouse CRP is

synthesized only in trace amounts unlike its human counterpart [28]. In addition, both SAA and CRP are used as an index for adverse prognosis of breast cancer [29]. Therefore, we believe that these diagnostic systems using acute phase proteins for human health would be useful for predicting the risk of exposure to nanomaterials as well as their likely toxicities. In addition, we showed that the induction time for the maximum level of haptoglobin, SAA and CRP are different after treatment with the silica nanoparticles (Figs. 2 and 3). Therefore, the predictive quality of these biomarkers is improved when they are used in combination.

Epidemiological studies have suggested that increased levels of ambient particle including particle with nanometer size are associated with adverse effects in the respiratory and cardiovascular systems [30]. Some reports have shown that humans exposed to ambient particle have increased blood levels of CRP [31]. In addition, epidemiological studies have shown associations between increased concentrations of SAA and CRP in plasma, and increased risk of cardiovascular diseases [32] and cancer [33]. Therefore we consider that acute phase proteins would be biomarkers for predicting the risk of inflammatory disease, cardiovascular diseases and cancer after exposure by nanomaterials.

In recent years there has been increasing use of nanomaterials in cosmetics, due to their light-diffusing properties and absorbencies, as well as in foodstuffs, such as additives in powdered foods. In particular, silica particles have been extensively used in many consumer products. For example, in the US, the use of amorphous silica is limited to less than 2.0% by weight of common salt. Other limits are defined for finished foods (<1%) and dried egg products (<5%). We cannot avoid exposure to nanomaterials, either from the unintentional release of waste products into the environment or by exposure to medicines, cosmetics and foodstuffs. Thus, it is important to carry out a safety analysis of nanomaterials after exposure *via* various routes. In this study, we showed that the level of acute phase proteins in the plasma of mice treated with nSP30 intranasally was elevated, although nSP70 did not induce elevation of each acute phase protein (Fig. 4). Therefore we consider that nSP30 would induce any toxic biological effects after intranasally treatment. Now we are trying to examine the pharmacokinetics and biological effects of nSP30 after intranasally treatment.

We then examined the effects of surface modification of silica nanoparticles on the production of acute phase proteins, because it has become evident that surface properties are important factors in the biological effects of particles. We showed that nSP70 with amino or carboxyl group surface modifications did not induce the production of each acute phase proteins (Fig. 5). Previously, we showed that surface modification of silica particles with functional groups such as amino or carboxyl group suppressed toxic biological effects of silica particles such as inflammatory responses [23]. These results also suggest that acute phase proteins could be a promising candidate biomarker for predicting the strength of toxicity induced by silica nanoparticles, although it is need to examine the toxic biological effects of silica nanoparticles with functional groups. Over recent years, nanomaterials have been introduced into our everyday lives. For example, silica particles, titanium dioxide and fullerenes of various crystallographic structures and surface functional groups are used in a range of different consumer products. Therefore, we are now trying to evaluate the response of acute phase proteins to exposure from various nanomaterials.

In general, acute phase proteins are known to be released from the liver mainly as a result of inflammatory cytokines such as interleukin (IL)-6 [19]. However, we confirmed that the levels of IL-6 were not elevated in the plasma of mice treated with silica particles at 24 h after treatment (data not shown). Therefore it is unclear why nanomaterials induce the production of acute phase proteins. We already showed that although silica particles with micrometer size tend to be taken up by Kupffer cells, silica nanoparticles with small particle sizes distribute around hepatic parenchymal cells (unpublished data). It is conceivable that instead of inflammatory cytokines, small silica particles act directly on the liver to induce the release of acute phase proteins. We are currently analyzing the detailed mechanism by which silica particles induce acute phase proteins in order to identify additional protein biomarkers.

5. Conclusions

We show here that acute phase proteins such as haptoglobin, CRP and SAA can act as useful biomarkers for analyzing the risk of exposure to nanomaterials and their associated toxicity. We believe that such information would be vital for the future development of predictive tests for estimation of the potential toxicity of new nanomaterials based on their physiochemical characteristics.

Acknowledgements

This study was supported in part by Grants-in-Aid for Scientific Research from the Ministry of Education, Culture, Sports, Science and Technology of Japan, and from the Japan Society for the Promotion of Science (JSPS). This study was also supported in part by Health Labour Sciences Research Grants from the Ministry of Health, Labor and Welfare of Japan; by Health Sciences Research Grants for Research on Publicly Essential Drugs and Medical Devices from the Japan Health Sciences Foundation; by a Global Environment Research Fund from Minister of the Environment; and by a the Knowledge Cluster Initiative; and by The Nagai Foundation Tokyo; and by The Cosmetology Research Foundation; and by The Smoking Research Foundation.

References

[1] Rutherglen C, Burke P. Nanoelectromagnetics: circuit and electromagnetic properties of carbon nanotubes. Small 2009;5:884–906.
[2] Kaur IP, Agrawal R. Nanotechnology: a new paradigm in cosmeceuticals. Recent Pat Drug Deliv Formul 2007;1:171–82.
[3] Cormode DP, Jarzyna PA, Mulder WJ, Fayad ZA. Modified natural nanoparticles as contrast agents for medical imaging. Adv Drug Deliv Rev 2010;62:329–38.
[4] Nel A, Xia T, Madler L, Li N. Toxic potential of materials at the nanolevel. Science 2006;311:622–7.
[5] Donaldson K, Murphy FA, Duffin R, Poland CA. Asbestos, carbon nanotubes and the pleural mesothelium: a review of the hypothesis regarding the role of long fibre retention in the parietal pleura, inflammation and mesothelioma. Part Fibre Toxicol 2010;7:5.
[6] Shvedova AA, Kagan VE, Fadeel B. Close encounters of the small kind: adverse effects of man-made materials interfacing with the nano-cosmos of biological systems. Annu Rev Pharmacol Toxicol 2010;50:63–88.
[7] Poland CA, Duffin R, Kinloch I, Maynard A, Wallace WA, Seaton A, et al. Carbon nanotubes introduced into the abdominal cavity of mice show asbestos-like pathogenicity in a pilot study. Nat Nanotechnol 2008;3:423–8.
[8] Morishige T, Yoshioka Y, Tanabe A, Yao X, Tsunoda S, Tsutsumi Y, et al. Titanium dioxide induces different levels of IL-1beta production dependent on its particle characteristics through caspase-1 activation mediated by reactive oxygen species and cathepsin B. Biochem Biophys Res Commun 2010; 392:160–5.
[9] Hougaard KS, Jackson P, Jensen KA, Sloth JJ, Loschner K, Larsen EH, et al. Effects of prenatal exposure to surface-coated nanosized titanium dioxide (UV–Titan). A study in mice. Part Fibre Toxicol 2010;7:16.
[10] Nishimori H, Kondoh M, Isoda K, Tsunoda S, Tsutsumi Y, Yagi K. Silica nanoparticles as hepatotoxicants. Eur J Pharm Biopharm 2009;72:496–501.
[11] Nishimori H, Kondoh M, Isoda K, Tsunoda S, Tsutsumi Y, Yagi K. Histological analysis of 70-nm silica particles-induced chronic toxicity in mice. Eur J Pharm Biopharm 2009;72:626–9.
[12] Nishimori H, Kondoh M, Isoda K, Tsunoda S, Tsutsumi Y, Yagi K. Influence of 70 nm silica particles in mice with cisplatin or paraquat-induced toxicity. Pharmazie 2009;64:395–7.
[13] Casado B, Iadarola P, Luisetti M, Kussmann M. Proteomics-based diagnosis of chronic obstructive pulmonary disease: the hunt for new markers. Expert Rev Proteomics 2008;5:693–704.

[14] Ferte C, Andre F, Soria JC. Molecular circuits of solid tumors: prognostic and predictive tools for bedside use. Nat Rev Clin Oncol; 2010 Jun 15 [Epub ahead of print].
[15] Vaidya VS, Ozer JS, Dieterle F, Collings FB, Ramirez V, Troth S, et al. Kidney injury molecule-1 outperforms traditional biomarkers of kidney injury in preclinical biomarker qualification studies. Nat Biotechnol 2010;28:478–85.
[16] Ozer JS, Dieterle F, Troth S, Perentes E, Cordier A, Verdes P, et al. A panel of urinary biomarkers to monitor reversibility of renal injury and a serum marker with improved potential to assess renal function. Nat Biotechnol 2010;28:486–94.
[17] Villota R, Hawkes JG. Food applications and the toxicological and nutritional implications of amorphous silicon dioxide. Crit Rev Food Sci Nutr 1986;23:289–321.
[18] Merget R, Bauer T, Kupper HU, Philippou S, Bauer HD, Breitstadt R, et al. Health hazards due to the inhalation of amorphous silica. Arch Toxicol 2002;75:625–34.
[19] Gabay C, Kushner I. Acute-phase proteins and other systemic responses to inflammation. N Engl J Med 1999;340:448–54.
[20] He X, Nie H, Wang K, Tan W, Wu X, Zhang P. In vivo study of biodistribution and urinary excretion of surface-modified silica nanoparticles. Anal Chem 2008;80:9597–603.
[21] Nabeshi H, Yoshikawa T, Matsuyama K, Nakazato Y, Arimori A, Isobe M, et al. Size-dependent cytotoxic effects of amorphous silica nanoparticles on Langerhans cells. Pharmazie 2010;65:199–201.
[22] Yamashita K, Yoshioka Y, Higashisaka K, Morishita Y, Yoshida T, Fujimura M, et al. Carbon nanotubes elicit DNA damage and inflammatory response relative to their size and shape. Inflammation 2010;33:276–80.
[23] Morishige T, Yoshioka Y, Inakura H, Tanabe A, Yao X, Narimatsu S, et al. The effect of surface modification of amorphous silica particles on NLRP3 inflammasome mediated IL-1beta production, ROS production and endosomal rupture. Biomaterials; 2010 Jun 17 [Epub ahead of print].
[24] Baumann H, Gauldie J. The acute phase response. Immunol Today 1994;15:74–80.
[25] Kushner I. The phenomenon of the acute phase response. Ann N Y Acad Sci 1982;389:39–48.
[26] Firpo MA, Gay DZ, Granger SR, Scaife CL, DiSario JA, Boucher KM, et al. Improved diagnosis of pancreatic adenocarcinoma using haptoglobin and serum amyloid A in a panel screen. World J Surg 2009;33:716–22.
[27] Korantzopoulos P, Kalantzi K, Siogas K, Goudevenos JA. Long-term prognostic value of baseline C-reactive protein in predicting recurrence of atrial fibrillation after electrical cardioversion. Pacing Clin Electrophysiol 2008;31:1272–6.
[28] Szalai AJ, McCrory MA. Varied biologic functions of C-reactive protein: lessons learned from transgenic mice. Immunol Res 2002;26:279–87.
[29] Pierce BL, Neuhouser ML, Wener MH, Bernstein L, Baumgartner RN, Ballard-Barbash R, et al. Correlates of circulating C-reactive protein and serum amyloid A concentrations in breast cancer survivors. Breast Cancer Res Treat 2009;114:155–67.
[30] Mauderly JL, Chow JC. Health effects of organic aerosols. Inhal Toxicol 2008;20:257–88.
[31] Ruckerl R, Ibald-Mulli A, Koenig W, Schneider A, Woelke G, Cyrys J, et al. Air pollution and markers of inflammation and coagulation in patients with coronary heart disease. Am J Respir Crit Care Med 2006;173:432–41.
[32] Albert MA, Ridker PM. The role of C-reactive protein in cardiovascular disease risk. Curr Cardiol Rep 1999;1:99–104.
[33] Siemes C, Visser LE, Coebergh JW, Splinter TA, Witteman JC, Uitterlinden AG, et al. C-reactive protein levels, variation in the C-reactive protein gene, and cancer risk: the Rotterdam Study. J Clin Oncol 2006;24:5216–22.

Biomaterials 32 (2011) 2713–2724

Contents lists available at ScienceDirect

Biomaterials

journal homepage: www.elsevier.com/locate/biomaterials

Systemic distribution, nuclear entry and cytotoxicity of amorphous nanosilica following topical application

Hiromi Nabeshi [a,b,1], Tomoaki Yoshikawa [a,b,1,*], Keigo Matsuyama [a,b], Yasutaro Nakazato [a,b], Kazuhiko Matsuo [c], Akihiro Arimori [a,b], Masaaki Isobe [a,b], Saeko Tochigi [a,b], Sayuri Kondoh [a,b], Toshiro Hirai [a,b], Takanori Akase [a,b], Takuya Yamashita [a,b], Kohei Yamashita [a,b], Tokuyuki Yoshida [a,b], Kazuya Nagano [b], Yasuhiro Abe [b], Yasuo Yoshioka [b,d], Haruhiko Kamada [b,d], Takayoshi Imazawa [e], Norio Itoh [a], Shinsaku Nakagawa [c], Tadanori Mayumi [f], Shin-ichi Tsunoda [b,g], Yasuo Tsutsumi [a,b,d,*]

[a] Department of Toxicology and Safety Science, Graduate School of Pharmaceutical Sciences, Osaka University, 1-6 Yamadaoka, Suita, Osaka 565-0871, Japan
[b] Laboratory of Biopharmaceutical Research (Pharmaceutical Proteomics), National Institute of Biomedical Innovation, 7-6-8 Saito-Asagi, Ibaraki, Osaka 567-0085, Japan
[c] Department of Biotechnology and Therapeutics, Graduate School of Pharmaceutical Sciences, Osaka University, 1-6 Yamadaoka, Suita, Osaka 565-0871, Japan
[d] The Center for Advanced Medical Engineering and Informatics, Osaka University, 1-6 Yamadaoka, Suita, Osaka 565-0871, Japan
[e] Bioresources Research, Laboratory of Common Apparatus, National Institute of Biomedical Innovation, 7-6-8 Saito-Asagi, Ibaraki, Osaka 567-0085, Japan
[f] Graduate School of Pharmaceutical Sciences, Kobe-Gakuin University, 1-1-3 Minatojima, Chuo-ku, Kobe, Hyogo 650-8586, Japan
[g] Department of Biomedical Innovation, Graduate School of Pharmaceutical Sciences, Osaka University, 7-6-8 Saito-Asagi, Ibaraki, Osaka 567-0085, Japan

ARTICLE INFO

Article history:
Received 12 October 2010
Accepted 27 December 2010
Available online 22 January 2011

Keywords:
Nanoparticles
Silica
Transdermal penetration
Cytotoxicity
Mutagenicity

ABSTRACT

Currently, nanomaterials (NMs) with particle sizes below 100 nm have been successfully employed in various industrial applications in medicine, cosmetics and foods. On the other hand, NMs can also be problematic in terms of eliciting a toxicological effect by their small size. However, biological and/or cellular responses to NMs are often inconsistent and even contradictory. In addition, relationships among NMs physicochemical properties, absorbency, localization and biological responses are not yet well understood. In order to open new frontiers in medical, cosmetics and foods fields by the safer NMs, it is necessary to collect the information of the detailed properties of NMs and then, build the prediction system of NMs safety. The present study was designed to examine the skin penetration, cellular localization, and cytotoxic effects of the well-dispersed amorphous silica particles of diameters ranging from 70 nm to 1000 nm. Our results suggested that the well-dispersed amorphous nanosilica of particle size 70 nm (nSP70) penetrated the skin barrier and caused systemic exposure in mouse, and induced mutagenic activity *in vitro*. Our information indicated that further studies of relation between physicochemical properties and biological responses are needed for the development and the safer form of NMs.

1. Introduction

A nanomaterial (NM) is defined as a substance that has at least one dimension of less than 100 nm in size. NMs can assume many different forms, such as tubes, rods, wires, spheres or particles. NMs have been widely used in consumer and industrial applications, such as medicine, cosmetics and foods, because they exhibit unique physicochemical properties and innovative functions [1]. However, NMs can also be problematic in terms of eliciting a toxicological effect by their small size. For example, exposure of cells or animals to carbon nanotubes, titanium dioxide nanoparticles or silver nanoparticles can induce cytotoxicity and inflammation [2–14]. We have previously shown that nSPs display a different intracellular localization compared with submicron- and micro-sized silica particles, and induce a greater cytotoxic response [15]. Whereas other studies reported that carbon nanotubes and titanium dioxide nanoparticles do not induce harmful effects [16–18]. Thus, despite intensive research efforts, reports of biological and/or cellular responses to NMs are often inconsistent and even contradictory. In addition, relationships among NMs physicochemical properties, absorbency, localization and biological responses are not yet well understood. In order to ensure the safety of NMs and open new frontiers in biological fields by the use of NMs, it is necessary to

* Corresponding authors. Department of Toxicology and Safety science, Graduate School of Pharmaceutical Sciences, Osaka University, 1-6 Yamadaoka, Suita, Osaka 565-0871, Japan. Tel.: +81 6 6879 8230; fax: +81 6 6879 8234.
E-mail addresses: tomoaki@phs.osaka-u.ac.jp (T. Yoshikawa), ytsutsumi@phs.osaka-u.ac.jp (Y. Tsutsumi).
[1] These authors contributed equally to the work.

0142-9612/$ – see front matter © 2011 Elsevier Ltd. All rights reserved.
doi:10.1016/j.biomaterials.2010.12.042

collect the information of the detailed properties of NMs from the point of view of biosafety and then, build comprehensive prediction system of NMs safety.

Accordingly, in this study, we evaluated the absorption properties and intracellular distribution of NMs, using typical NMs, amorphous nanosilica particles (nSP) and quantum dots (QD). nSP are one of the most widely applied NMs, and are used in cosmetics and food additives. nSPs and QD also have great potential for use as diagnostic imaging agents, gene delivery carriers and cancer therapies [19–23]; in addition, these NMs show overwhelmingly superior dispersibility as compared with carbon nanotubes, fullerene and nano-sized titanium dioxide (TiO_2). Thus, these NMs are ideally suited for determining how particle size influences the biodistribution and biological effects of NMs.

2. Materials and methods

2.1. Silica particles

Suspensions of fluorescent (red-F)-labeled amorphous silica particles (Micromod Partikeltechnologie GmbH) (25 mg/ml and 50 mg/ml) were used in this study; particle size diameters were 70, 300 and 1000 nm (designated as nSP70, nSP300 and mSP1000, respectively). Silica particles were used following 5 min sonication and 1 min vortex.

2.2. Quautum dots

Quantum dots (QD) with emission maxima at 565 nm were obtained from Invitrogen (Hayward, CA). They were sold as Qtracker® Non-targeted Quantum Dots (PEG). QD were used after 5 min sonication and 1 min vortex.

2.3. Animals

BALB/c mice (female, 6–8 weeks) were purchased from Japan SLC, Inc. Mice were housed in a ventilated animal room maintained at 20 ± 2 °C with a 12-h light/12-h dark cycle. Mice had free access to water and alfalfa-free forage (FR-2, Funabashi farm). The experimental protocols conformed to the ethical guidelines of the National Institute of Biomedical Innovation.

2.4. Cell culture

HaCaT human keratinocyte cell line was kindly provided by Dr. Inui, Osaka University. HaCaT cells were cultured in Dulbecco's modified Eagle's medium (D-MEM) supplemented with 10% heat-inactivated fetal bovine serum and 0.2 mM L-glutamine. The cells were grown in a humidified incubator at 37 °C (95% room air, 5% CO_2).

2.5. Physicochemical examinations of silica particles and QD

Silica particles and QD were diluted to 0.25 mg/ml (nSP70), 0.5 mg/ml (nSP300 and mSP1000) or 0.5 μM (QD) with PBS, respectively and the average particle size and zeta potential were measured using the Zetasizer Nano-ZS (Malvern Instruments Ltd). The mean size and the size distribution of silica particles were measured by dynamic light scattering method. The zeta potential was measured by laser Doppler electrophoresis. pH of each particles suspension were measured by ISFET-pH meter (SHINDENGEN, Japan). The size and shape of silica particles and QD were observed using transmission electron microscopy (TEM). Prior to TEM analysis, nSP70 were stained with 2% uranium acetate and QD were enhanced by silver using a standard AURION R-GENT SE-EM regent and protocol.

2.6. Dermal administration of silica particles and transmission electron microscopy (TEM) analysis of skin, lymph node and liver

nSP70 (250 μg/ear/day) and QD (1.2 pmol/ear/day) suspension supplemented with 10% isopropyl myristate were applied to the inner side of both ears of BALB/c mice for 28 days. In both samples, the total number of particles applied over 28 days was 2.8×10^{13} particles. After 24 h of last administration, skin, lymph node and brain from each mouse were excised and fixed in 2.5% glutaraldehyde for 2 h. Then, small pieces of tissue sample were washed with phosphate buffer three times and post-fixed in sodium cacodylate-buffered 1.5% osmium tetroxide for 60 min at 4 °C, block stained in 0.5% uranyl acetate, dehydrated by dipping each of them through a series of ethanol solutions containing increasing concentration of ethanol, and embedded in Epon resin (TAAB). Ultrathin sections were stained with uranyl acetate and lead citrate (silica particles-treated samples) or AURION R-GENT SE-EM regent (QD-treated samples). The stained samples were subsequently observed under a Hitachi electron microscope (H-7650).

2.7. Detection of apoptotic cells in the nSP70-applied mice skin (terminal deoxynucleotidyl transferase-mediated X-dUTP nick-end labeling (TUNEL) staining)

The TUNEL staining was performed on paraffin-embedded skin sections of 28-day application of nSP70. The skin was fixed in 10% neutral buffered formalin and then embedded in paraffin. Paraffin-embedded skin was sliced and placed on glass slides. DNA strand breaks, which are associated with the apoptotic response, were detected with an *in situ* Cell Death Detection Kit, TMR red (Roche) according to protocol of this kit. Deparaffinization and rehydration of the skin sections were carried out according to standard protocols. Then, the skin sections were incubated with proteinase K for 30 min. After rinse of the skin sections twice with PBS, 50 μl of TUNEL reaction mixture were added on the skin sections and incubated for 60 min at 37 °C in the dark. The skin sections were rinsed 3 times with PBS and mounted with the mounting agent, ProLong Gold Antifade Reagent with DAPI (Invitrogen). The skin sections were analyzed under a fluorescence microscope (BIOREVO, KEYENCE) with excitation wavelength in the range of 520–560 nm and detection in the range of 570–620 nm. For counting the numbers of TUNEL-positive cells, approximately 1000 cells were randomly selected from 3 different areas in each section and examined under a fluorescence microscope at magnification of ×200.

2.8. Transmission electron microscopy (TEM) analysis of human keratinocyte cells

HaCaT cells were cultured in the presence of various sized silica particles (100 μg/ml) for 24 h on chamber slides, and then fixed in 2.5% glutaraldehyde followed by 1.5% osumium tetraoxide. The fixed cells were dehydrated and embedded in EPON resin. Ultrathin sections were stained with lead citrate and observed under an electron microscope.

2.9. Evaluation of the proliferation of silica particle- or QD-treated cells (^{3}H-thymidine incorporation assay)

Proliferation of silica particle- or QD-treated HaCaT cells was measured by ^{3}H-thymidine incorporation assay. 1×10^4 cells were cultured with varying concentrations of silica particles or QDs for 18 h at 37 °C and ^{3}H-thymidine (1 μCi/well) was then added into each well. After a further 6 h, cells were harvested and lysed on glass fiber filter plates using a Cell harvester (PerkinElmer). The filter plates were then dried and counted by standard liquid scintillation counting techniques in a Top-Counter (PerkinElmer).

2.10. Mutagenicity assay (Ames test)

The mutagenicity assay was performed to evaluate the intrinsic mutagenic potency of the silica particles. For this purpose, the *Salmonella typhimurium* (*S. typhimurium*) mutagenicity test was performed according to the method of Ames [24–26]. Two strains of *S. typhimurium* bacteria were used, namely, TA98 and TA100. Experiments were conducted according to guideline of Health, Labour and Welfare Ministry. The test was carried out using 100 μl of well-dispersed solutions (10, 90, and 810 μg/ml) of silica particles. 2-Aminofluorene (2-AF) dissolved in DMSO was used as a positive control for the mutagenicity assay.

2.11. Determination of DNA damage (comet assay)

Damage of endogenous DNA in HaCaT cells after treatment with a given silica particles were analyzed by alkaline comet assay according to the Comet Assay Kit (Trevigen). All steps were conducted under dim yellow light to prevent additional DNA damage. Briefly, 3×10^4 HaCaT cells were seeded into each well of a 6-well plate and incubated for 24 h. After 24 h, cells were treated with 30 or 90 μg/ml nSP70, nSP300, mSP1000 or 0.2 mM H_2O_2 (positive control) or PBS (negative control) for 3 h. Cells from each group were resuspended at a density of 1×10^5 cells/ml in ice cold CMF-PBS and combined with molten LM Agarose (Trevigen) at a ratio of 1:10 (v/v). The cell-agarose mixture was immediately pipetted onto a frosted microscope slide (CometSlide; Trevigen). Each slide was then placed flat at 4 °C in the dark for 60 min, immersed in prechilled lysis solution (Trevigen), and left at 4 °C for 40 min to remove cellular proteins, leaving the DNA molecules exposed. The slides were then immersed in an alkaline solution (pH > 13, 0.3 M NaOH and 1 mM EDTA) for 40 min to denature the DNA and hydrolyze the sites that were damaged. The samples were electrophoresed for 10 min and stained with SYBR green I (Trevigen) according to the manufacturers instructions. Twenty-five cells on each slide, randomly selected by fluorescence microscopy, were then analyzed using the Comet Analyzer (Youworks Corporation).

2.12. In vivo imaging

Biodistribution of fluorescent-labeled silica particles was analyzed in live mice and excised tissues using the IVIS 200 imaging system (Xenogen corp.). Three female Hos: HR-1 mice were treated with 100 mg/kg DY-676 (excitation (ex) and emission (em) wavelengths 674 and 699 nm, respectively)-labeled silica particles of each particle size (70, 300 and 1000 nm) by intravenous injection. After anesthesia with isoflurane, live mouse fluorescence optical imaging was performed using the cy5.5

filter set (ex/em 615-665/695-770). Tissues were then excised from the mice and fluorescent images of the tissues were obtained. Imaging parameters were selected and implemented using the instrument, Living Image 2.5 software. Bright field photographs were obtained for each imaging time. The merged bright field photographs and fluorescent images were generated using Living Image 2.5 software.

2.13. Transmission electron microscopy (TEM) analysis of liver

BALB/c mice were treated with 0.6 mg/mouse (about 30 mg/kg, 70 nm) or 2 mg/mouse (about 100 mg/kg, 300 and 1000 nm) silica particles of each particle size and PBS (control) by intravenous injection. After 24 h, the tissues and organs such as brain, heart, lung, liver, kidney, spleen and lymph node, were excised and fixed in 2.5% glutaraldehyde for 2 h. Small pieces of tissue sample were then washed with phosphate buffer three times and postfixed in sodium cacodylate-buffered 1.5% osmium tetroxide for 60 min at 4 °C, block stained in 0.5% uranyl acetate, dehydrated through a series of ethanol concentrations, and embedded in Epon resin (TAAB). Ultrathin sections were stained with uranyl acetate and lead citrate. The samples were examined under a Hitachi electron microscope (H-7650).

2.14. Living cell counting and DNA damage determination in isolated primary hepatocytes from silica particle-treated mice

Female BALB/c mice were treated with 2 mg/mouse (about 100 mg/kg) silica particles of each particle size (70, 100, 300 and 1000 nm) and PBS (control) by intravenous injection. After 5 h, parenchymal hepatocytes were isolated according to the *in situ* two-step collagenase perfusion technique. Briefly, the liver was perfused with 25 ml of 10 mM Hepes buffered calcium- and magnesium-free Hanks' balanced salt solution (HBSS) containing 190 mg/l EGTA (DOJINDO) for 5 min. The liver was then perfused with 40 ml of HBSS containing 250 mg/l trypsin inhibitor, 500 mg/l collagenase and 550 mg/l $CaCl_2$ for 10 min. The liver was then excised and the cells dispersed in HBSS. The cells were then centrifuged at 50 × g at 4 °C for 1 min. The resulting pellet was resuspended in 20 ml of L15 medium containing 5% FCS, 1 μM dexamethasone and 1 μM insulin and centrifuged at 50 × g at 4 °C for 1 min. This step was repeated 3 times. The resulting pellet was resuspended in medium and living cells were counted using trypan blue staining. Endogenous DNA damage in isolated primary parenchymal hepatocytes from mice treated with nSP70, nSP300, mSP1000 and PBS (control) was analyzed by alkaline comet assay as described above.

2.15. Statistical analysis

Statistical comparisons between groups were performed by one-way ANOVA with Bonferroni test as a *post hoc* test. The level of significance was set at $P < 0.05$.

3. Results and discussion

3.1. Physicochemical properties of various sized silica particles and QD

The first step for ensuring the biosafety of NMs are to evaluate whether the NMs could penetrate the epithelial barriers, could eventually become absorbed systemically, and more importantly, whether they could be responsible for acute/chronic side effects. In this context, here, we evaluated whether the nSP and QD could penetrate into the skin of BALB/c mice following dermal exposure. Prior to undertaking the skin penetration study, we first analyzed the physicochemical properties of the commercially available silica particles of 70, 300 and 1000 nm in diameter (nSP70, nSP300 and mSP1000, respectively). Close examination of the silica particles of different particle sizes by TEM revealed that all silica particles used in this study were smooth-surfaced spherical particles and in size category the primary particle sizes were approximately uniform (Fig. 1a–f). According to technical datasheet, surface textures of all silica particles were plain and nonporous. The specific surface area was calculated by means of the following equation; $s = 6/d\rho$ (where s, specific surface area (m^2/g); ρ, density (g/cc); d, diameter (μm)). The specific surface area of nSP70, nSP300 and mSP1000 calculated using this equation was 43, 10 and 3 m^2/g, respectively. In addition, all silica particles used in this study was not modified with any functional groups. These physicochemical properties were summarized in Table 1. From the results of mean particle size in solution, it was suggested that the silica particles used in this study remained as stable well-dispersed particles in solution, and not as aggregates. Thus, these particles are ideally suited as optimal sample to evaluate if and whether their biodistribution and biological effect depend on the particle size. As well as silica particles, the shape, size distribution and zeta potential of QD were evaluated. Surface of QD used in this study were coated with polyethylene glycol (PEG). QD were enhanced using silver for TEM analysis, because silver selectively deposits on the QD [27]. From the results of TEM analysis, QD were also spherical particles, and in terms of size category the primary particle sizes (about 35 nm) were approximately uniform. The size distribution spectrum of QD in a neutral solvent showed two peaks, and the average particle size of peaks 1 and 2 was about 35 and 300 nm, respectively.

3.2. Analysis of transdermal penetration and biodistribution of nanosilica and QD applied on the skin

We next used TEM to determine whether nSP with a particle size below 100 nm would penetrate the skin after topical application. As a result, the 28-day application of nSP70 to mice showed that nSP70 entered not only the skin (Fig. 2a), the regional lymph nodes (Fig. 2b) and the parenchymal hepatocytes present in liver (Fig. 2c, d) but also the cerebral cortex (Fig. 2e) and the hippocampus (Fig. 2f). Surprisingly, penetration of nSP70 into the liver was also detected, and some of the nSP70 that entered the parenchymal hepatocytes were found to be distributed throughout the cytoplasm and inside the nucleus (Fig. 2c) and mitochondria (Fig. 2d). Localization of nSP70 in the nucleus was also detected in the skin and the lymph node (Fig. 2a, b). Next, the skin permeability of QD was evaluated. We found that QD penetrated the stratum corneum and entered the skin (Fig. 2g), lymph node (Fig. 2h), liver (Fig. 2i, j), cerebral cortex (Fig. 2k) and hippocampus (Fig. 2l). In addition, some of the QD that entered the skin (Fig. 2g), lymph node (Fig. 2h) and parenchymal hepatocytes (Fig. 2i) were detected inside the nucleus, similar to nSP70. We considered that the well-dispersed portion of QD showed skin permeability. It has been reported that QD can enter the skin by transdermal exposure under ultraviolet radiation [27]. However, for the first time we have revealed that nSP and QD penetrate the skin and enter tissues such as the lymph node, liver and brain under normal conditions.

3.3. Analysis of biological effects induced by nanosilica and QD

The next step for the biosafety should include analyzing their biological effects against skin, brain, liver and lymph node. Consequently, first, in order to assess the biological response in the skin as a part of 28-day application of nSP70, we tried to detect the apoptotic cells by using Terminal Deoxynucleotidyl Transferase-Mediated X-dUTP Nick-End Labeling (TUNEL) staining. As a result, while a few TUNEL-positive cells were detected in water-applied mice skin (control) (Fig. 3a), a number of TUNEL-positive cells (expressed in red) were detected in nSP70-applied mice skin (Fig. 3b). The ratio of TUNEL-positive cells in the skin sections of mice transdermally-applied with nSP70 tended to increase compared to mice transdermally-applied with water (control). In one of two nSP70-applied mice, the ratio of TUNEL-positive cells in the skin section was dominantly increased (Fig. 3c). This result suggested that the transdermal application of nSP70 induced the cellular damage in the skin. On the basis of this result and transdermal absorption test results, we are now evaluating higher cerebral function, hepatic drug metabolism, and the immune system of mice after topical nSP exposure. Moreover, it is necessary to evaluate the influence of well-dispersed NMs on nuclear and mitochondrial functions, because we found that nSP70 and QD enter into these specific organelles. These results also suggest that systemic safety analysis (hazard analysis) of an NM is highly important for ensuring its safety. Because nSP70 and QD can

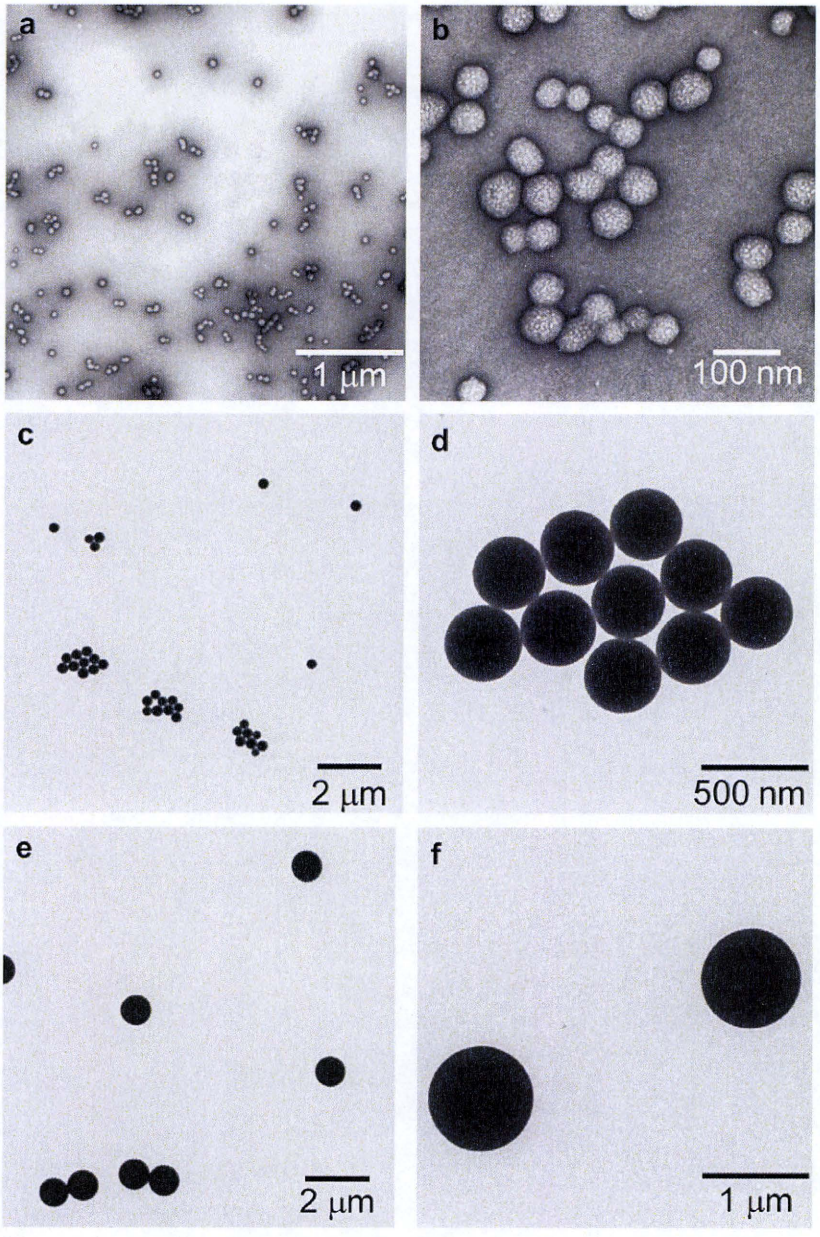

Fig. 1. Transmission electron microscopy (TEM) analysis of silica particles. a–f, TEM photomicrographs of silica particles used in this study: nSP70 (a and b), nSP300 (c and d) and mSP1000 (e and f). Each type of sized silica particles existed as scattered and spheroidal. Scale bars: 1 μm (a and f), 100 nm (b), 500 nm (d) and 2 μm (c and e).

penetrate the skin barrier, which is the most rigid biological barrier, we believe that analysis of oral and pulmonary exposure should also be included in ensuring the biosafety of NMs.

Collectively, these observations clearly show that nSPs and QD of less than 100 nm in diameter invade the body through the skin, suggesting that human beings are at high risk of exposure to NMs through the blood stream. Consequently, we analyzed the distribution and biological effects of NMs with a focus on the region level and the systemic level. Because nSPs have already been put into practical use in cosmetics, firstly, we evaluated the intracellular

Table 1
Summary of the physicochemical properties of silica particles.

	Primary particle size (nm)[a]	Hydrodynamic diameter (nm)	Mean zeta potential (mV)	pH	Surface texture[a]	Porosity[a]	Surface area (m^2/g)[b]	Functional group[a]
nSP70	70	77.0 ± 0.4	−21.6 ± 4.5	7.4	Plain	Nonporous	43	None
nSP300	300	269.3 ± 2.1	−31.3 ± 6.5	7.5	Plain	Nonporous	10	None
mSP1000	1000	1187 ± 25.2	−37.7 ± 4.6	7.9	Plain	Nonporous	3	None

Mean particle size and zeta potential in solution of silica particles are expressed as mean ± S.D. ($n = 3$).

[a] Information from technical datasheet of products.

[b] The specific surface area was calculated by means of the following equation; $s = 6/d\rho$ (where s, specific surface area (m^2/g); ρ, density (g/cc); d, diameter (μm)).

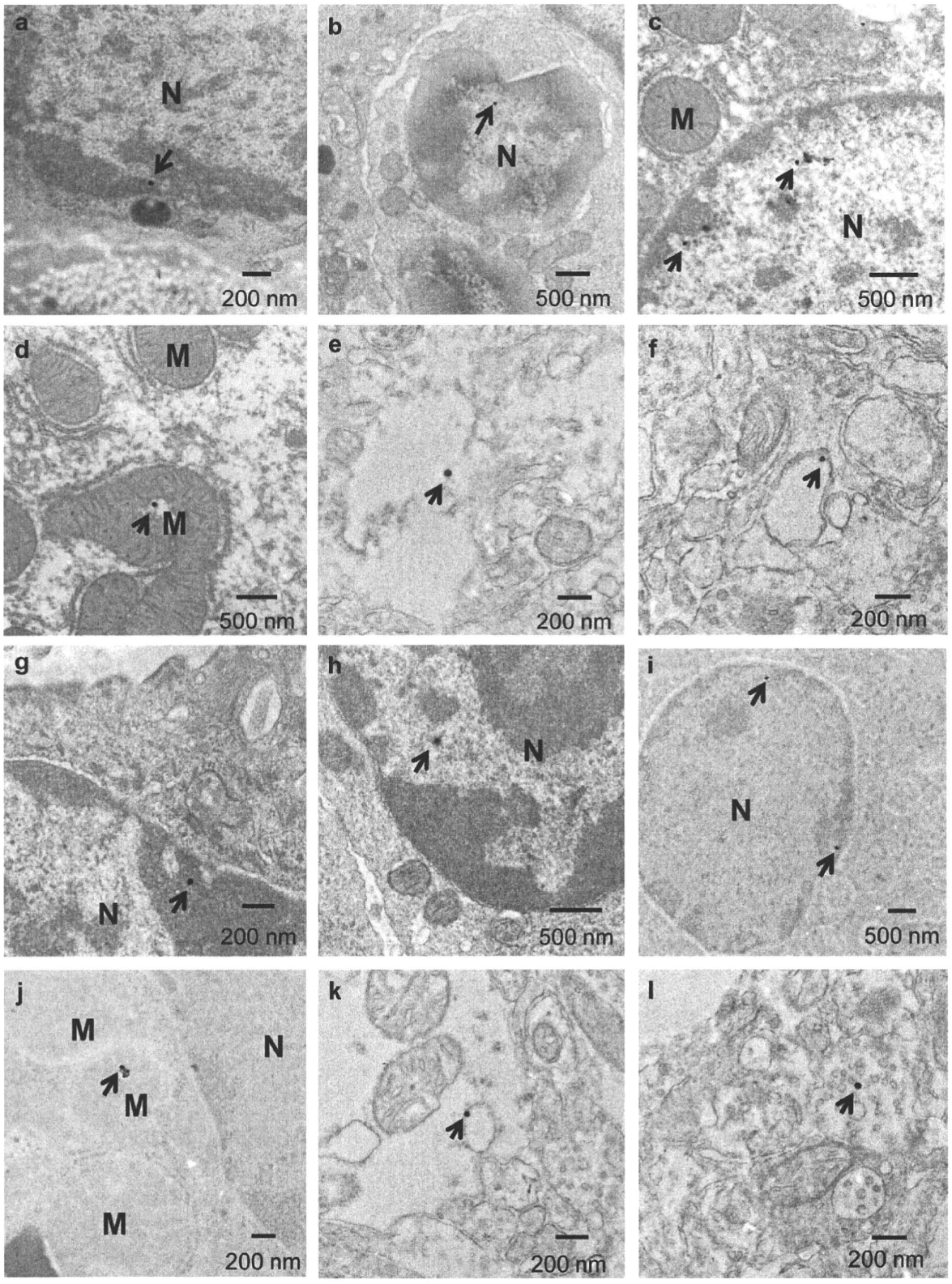

Fig. 2. TEM analysis of skin, lymph node, liver and brain samples from mice after 28-days of dermal exposure to silica nanoparticles and quantum dots. a–c, nSP70 (arrows) were present in the nucleus of skin (a), cervical lymph node (b), and parenchymal hepatocytes (c). d, nSP70 were also detected in the mitochondria of parenchymal hepatocytes. e–f, nSP70 were found in neuron of the cerebral cortex (e) and the hippocampus (f). g–h, QD (arrows) were present in the nucleus of skin (g), cervical lymph node (h) and parenchymal hepatocytes (i), similar to nSP70. j, In parenchymal hepatocytes, QD were detected in the mitochondria (j). k–l, QD were found in neuron of the cerebral cortex (k) and the hippocampus (l). N: nucleus; M: mitochondria. Scale bars: 200 nm (a, e–g, and j–l), 500 nm (b–d, h and i).

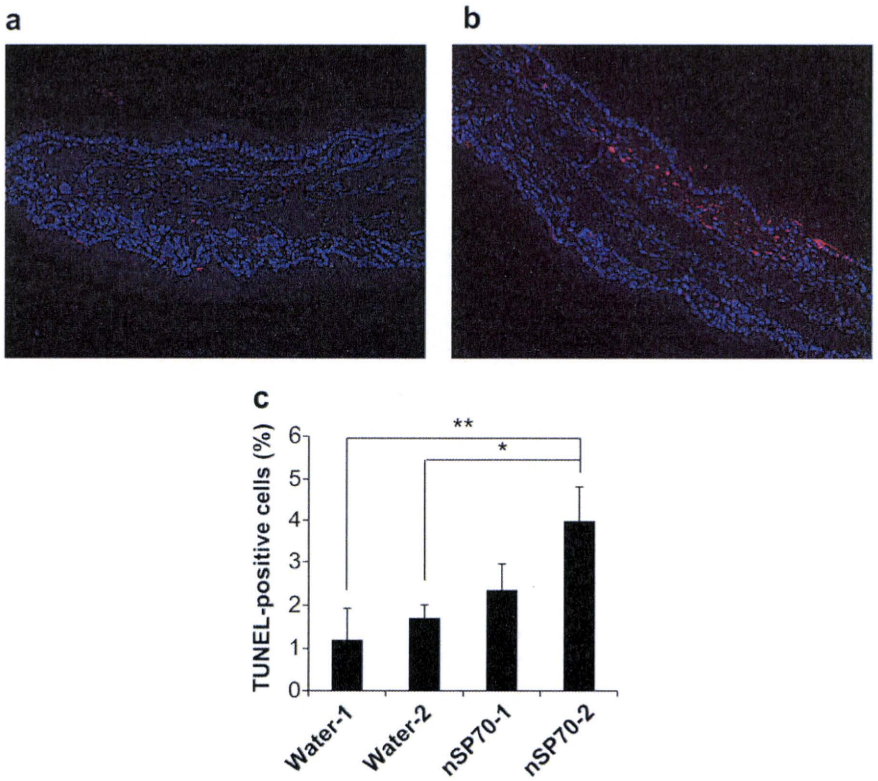

Fig. 3. Detection of apoptotic cells in silica nanoparticles-applied mice skin. a, b, Representative images from TUNEL stained skin section in water- (control, a) and nSP70- (b) applied mice were shown. Nuclei and TUNEL-positive cells were represented in blue and red, respectively. Original magnification, ×200. c, For quantification of TUNEL-positive cells, approximately 1000 cells were randomly selected from 3 different areas in each section and two animals and counted the numbers of positive cells expressed as a percentage of the total (c). Data shown are average means (±SD) of each treated group. * Significant increase ($P < 0.005$) compared with Water-2. ** Significant increase ($P < 0.001$) compared with Water-1.

distributions and biological responses of NM size in skin with a focus on nSP.

3.4. Analysis of intracellular distribution of silica particles in human keratinocyte

Presently, many modern cosmetic or sunscreen products contain nano-sized components, such as titanium dioxide (TiO_2), zinc oxide (ZnO) and amorphous silica particles. Nano-sized TiO_2 and ZnO are colorless substances and reflect/scatter ultraviolet (UV) more efficiently than their larger counterparts [28,29]. Amorphous nanosilica particles (nSPs) are used in large quantities and are one of the most important ingredients in the cosmetic industry, especially for their light-diffusing and absorption properties. Extensive consumption of these NM-supplemented cosmetic and food products has naturally raised the question as to whether these NMs could penetrate the skin, would eventually become absorbed systemically, and more importantly, whether they could be responsible for acute/chronic side effects. In the present study, we revealed that well-dispersed nSP could penetrate into and pass through the skin. Interestingly, we found that nSP70 migrated into the blood stream and passed into tissues such as liver. Moreover, nSP70 invaded specific organelles such as the nucleus and mitochondria. In view of these observations, we next examined the relation between the intracellular distribution and biological effects of nSP, which are the most important NMs in our daily life.

To determine the intercellular location of silica particles, we used TEM to examine the HaCaT cells that were treated with 100 μg/ml of nSP70, nSP300, or mSP1000. TEM examination revealed the presence of mSP1000 and nSP300 only in the endosome (Fig. 4a, b, arrows). mSP1000-treated cells were also found to contain a large number of lysosomes (Fig. 4a). In contrast, only in the nSP70-treated cells nSP70s were present in the cytoplasm as well as in the nucleus (Fig. 4c, d, arrow heads). Furthermore, nSP70s were accumulated in the nucleolus (Fig. 4e, f, arrows). Recently, it has been reported that the intercellular localization of NM is possibly linked to the induction of harmful effects. For example, the localization of silver nanoparticles in the nucleus and mitochondria may be related to mitochondrial dysfunction or oxidative stress [30]. Thus, analysis of intracellular localization enables us to provide important and useful information to predict the hazard to human health.

3.5. Analysis of cell-growth inhibition and genotoxicity induced by silica particles

Next, we investigated the biological effects of nSP. To this end, we assessed the effects of various particle size nSP on the proliferation of HaCaT cells. As shown in Fig. 5a, cell proliferation was inhibited following treatment with nSP70 and nSP300 in both dose and size dependent manner. The half maximal (50%) inhibitory concentration (IC_{50}) of nSP70 and nSP300 for inhibiting cell proliferation was 323 and 3966 μg/ml, respectively. We were, however, unable to calculate the IC_{50} of nSP1000. Taken together, these results suggested that smaller sized silica particles inhibited the growth of HaCaT cells more strongly than the larger particles. In addition, we assessed the effects of QD on the proliferation of HaCaT cells. As the result, we indicated that the effect to cell proliferation of QD was predominantly lower than nSP70 at same